Available online at www.sciencedirect.com
ScienceDirect
Geochimica et Cosmochimica Acta 72 (2008) 4069–4093
Geochimica et Cosmochimica Acta
www.elsevier.com/locate/gca

Evaluating transition-metal catalysis in gas generation from the Permian Kupferschiefer by hydrous pyrolysis

M.D. Lewan [a,*], M.J. Kotarba [b], D. Więcław [b], A. Piestrzyński [b]

[a] U.S. Geological Survey, Box 25046, MS 977, Denver Federal Center, Denver, CO 80225, USA
[b] AGH-University of Science and Technology, Al. Mickiewicza 30, 30-059 Krakow, Poland

Received 24 October 2007; accepted in revised form 5 June 2008; available online 14 June 2008

Abstract

Transition metals in source rocks have been advocated as catalysts in determining extent, composition, and timing of natural gas generation (Mango, F. D. (1996) Transition metal catalysis in the generation of natural gas. *Org. Geochem.* **24**, 977–984). This controversial hypothesis may have important implications concerning gas generation in unconventional shale-gas accumulations. Although experiments have been conducted to test the metal-catalysis hypothesis, their approach and results remain equivocal in evaluating natural assemblages of transition metals and organic matter in shale. The Permian Kupferschiefer of Poland offers an excellent opportunity to test the hypothesis with immature to marginally mature shale rich in both transition metals and organic matter. Twelve subsurface samples containing similar Type-II kerogen with different amounts and types of transition metals were subjected to hydrous pyrolysis at 330° and 355 °C for 72 h. The gases generated in these experiments were quantitatively collected and analyzed for molecular composition and stable isotopes. Expelled immiscible oils, reacted waters, and spent rock were also quantitatively collected. The results show that transition metals have no effect on methane yields or enrichment. $\delta^{13}C$ values of generated methane, ethane, propane and butanes show no systematic changes with increasing transition metals. The potential for transition metals to enhance gas generation and oil cracking was examined by looking at the ratio of the generated hydrocarbon gases to generated expelled immiscible oil (i.e., GOR), which showed no systematic change with increasing transition metals. Assuming maximum yields at 355 °C for 72 h and first-order reaction rates, pseudo-rate constants for methane generation at 330 °C were calculated. These rate constants showed no increase with increasing transition metals. The lack of a significant catalytic effect of transition metals on the extent, composition, and timing of natural gas generation in these experiments is attributed to the metals not occurring in the proper form or the poisoning of potential catalytic microcosms by polar-rich bitumen, which impregnates the rock matrix during the early stages of petroleum formation.
Published by Elsevier Ltd.

1. INTRODUCTION

Transition-metal catalysis in source rocks has been advocated as a critical mechanism in determining the extent, composition, and timing of natural gas generation (Mango, 1996). The significance of this mechanism remains controversial (e.g., Snowdon, 2001), but it may have important implications in assessing unconventional shale gas plays, with some reserve estimates in the range of multitrillions of cubic feet of gas (Montgomery et al., 2005). Although experiments have been conducted to test transition-metal catalysis, their approach and results remain equivocal in evaluating the mechanism in natural assemblages of transition metals and organic matter in shale. NiO dispersed on a silica gel is typically used as the catalyst in previous experiments with alkenes and H_2 yielding methane-enriched gas at 200 °C (Mango, 1996). However, NiO is a rare mineral (i.e., Bunsenite) in nature, and its absence in sedimentary rocks makes its relevance as a catalyst in nature during thermal maturation unlikely. Other

* Corresponding author. Fax: +1 303 236 3202.
E-mail address: mlewan@usgs.gov (M.D. Lewan).

0016-7037/$ - see front matter Published by Elsevier Ltd.
doi:10.1016/j.gca.2008.06.003

experiments used artificially matured source rocks (350 °C/24 h) as a catalyst with an alkene and H_2 to yield methane-enriched gas at 190 °C after several days (Mango, 1994). These results were interpreted as catalytic methane generation from the thermal decomposition of the extraneous alkene and H_2. However, it was not established whether the catalyst was transition metals, organic substrates, or minerals within the matured rock. Therefore, additional experiments are needed to better evaluate the significance of transition-metal catalysis in gas generation from petroleum source rocks.

The Permian Kupferschiefer of southwestern Poland offers an excellent opportunity to evaluate transition-metal catalysis in gas generation experiments. This rock unit contains immature to marginally mature shale rich in both transition metals and organic matter (Püttmann et al., 1991). World famous for its base-metal enrichment, this thin (<1 m) black shale contains transition-metal concentrations on the order of several weight percent (Kucha, 1993). Copper, lead, and zinc are the dominant transition metals, but high concentrations (>100 ppm) of other transition metals (e.g., Ni, V, Co, Mo, and Ag) also occur (Kucha and Mayer, 1996). Oszczepalski (1989) reports about 80% of the metals occur as fine-grained (<50 μm) disseminations in organic-rich portions of the shale matrix. The remaining 20% occur as coarse-grained (>100 μm) aggregates, lenses, or veinlets. Although sulfides host a large portion of the Cu, Pb, and Zn, some of the transition metals (e.g., Cu, Ni, V, Co, and Mo) are present in the organic matter as possible organometallic complexes (Hammer et al., 1988; Kucha, 1993; Sawłowicz, 1993). Another favorable attribute of these samples is their exceptionally high concentrations of Cu, which is a versatile transition metal for various industrial catalytic gas reactions involving methanol formation (Olah and Molnár, 2003, p. 114), oxidation of ethene (Somorjai, 1994, p. 460), ethene hydrogenation (Masel, 2001, p. 879), and ethane hydrogenolysis (Bond, 2005, p. 537).

The tenet of this study is that if transition-metal catalysis is an important mechanism, these exceptionally high concentrations of transition metals should show some effects on gas generation from the associated organic matter when subjected to laboratory pyrolysis. In this study, twelve immature to marginally mature subsurface samples containing similar Type-II kerogen with different amounts and types of transition metals were subjected to hydrous pyrolysis at 330 and 355 °C for 72 h. The gases generated in these experiments were quantitatively collected and analyzed for their molecular and stable isotopic compositions. Expelled immiscible oils, reacted waters, and spent rock were also quantitatively collected and analyzed. The objectives of the study are to evaluate whether transition metals in these samples have a catalytic effect on the yield, composition, and timing of gas generated by hydrous pyrolysis.

2. SAMPLES AND METHODS

2.1. Sample description

The 12 Kupferschiefer samples used in this study were collected on the basis of their low thermal maturity, high total organic carbon (TOC), similar Type-II kerogen, and varying amounts and types of transition metals. Specific locations for sampling were determined from a data base of more than 400 samples previously collected and analyzed for metal content, TOC, and Rock-Eval parameters for the Polish Copper Company KGHM Polska Miedź S.A. Sampling locations are shown in Fig. 1 and described in Table 1. The samples from the Polish Fore-Sedetic Monocline represent a wide range of types and quantities of transition metals with either Cu or Pb being the dominant ore metal. The German mine sample (Cu-Wett) was included because it contains Zn as the dominant ore mineral, with Cu and Pb occurring in subordinate concentrations. The Pomeranian core sample (Łeba-8) was included because it was never subjected to epigenetic mineralization and contains syngenetic metal assemblages typical of black shale. A minimum of 1 kg of each sample was collected, crushed, and sieved to gravel size (0.5–2.0 cm) for the experiments.

2.2. Experimental approach and collection procedures

Each experiment involved loading a 380-g aliquot of gravel-sized sample in a 1-l Hastelloy-C276 reactor (Parr 4653) with 400 g of distilled water. This water-to-rock proportion is based on calculations using steam tables and measured bulk rock densities to insure that the rock samples remain in contact with liquid water throughout the experiments (Lewan, 1993). The loaded reactor is sealed with a stainless steel-316 gasket and an 8-bolt split-ring head. The sealed reactor is pressurized to 6.9 MPa of helium and checked for leaks with a thermal conductivity gas-leak detector (Gow-Mac 21-250). The helium pressure is reduced to a pressure between 200 and 221 kPa. This pressure and the temperature are recorded, and based on the headspace volume, the millimoles of introduced He are calculated. The reactors are isothermally heated in electric heaters at 330.1 ± 0.2 or 355.1 ± 0.3 °C for 72.08 ± 0.04 h. Experimental duration was determined from the time the intended temperature was first reached to the time the temperature fell 0.5 °C below the intended temperature after the heater was turned off. Heat-up times to reach the intended temperature were 56 ± 6 min for 330 °C and 64 ± 0.8 min for 355 °C. After a reactor cooled to room temperature, it was weighed to within 0.1 g and compared with the preheated weight to determine whether or not leakage had occurred during heating. The average weight loss after heating was 0.5 ± 0.3 g, which is attributed to loss of volatiles from the anti-seize lubricant used on the closure head bolts during heating. The reactor is connected to a gas inlet system of known volume. The reactor headspace gas is slowly bled into the evacuated inlet system and a final pressure and temperature are recorded. Gas samples are then taken in two evacuated 30- or 50-cm^3 stainless steel cylinders for molecular and stable isotopic analyses. As previously described by Lewan (1993), the expelled immiscible oil on the water surface is quantitatively collected with a Pasteur pipette and a subsequent benzene rinse. The spent rock was recovered in a 150- × 20-cm Petri dish and allowed to dry under a fume hood until weights became constant, which typically took 4 days.

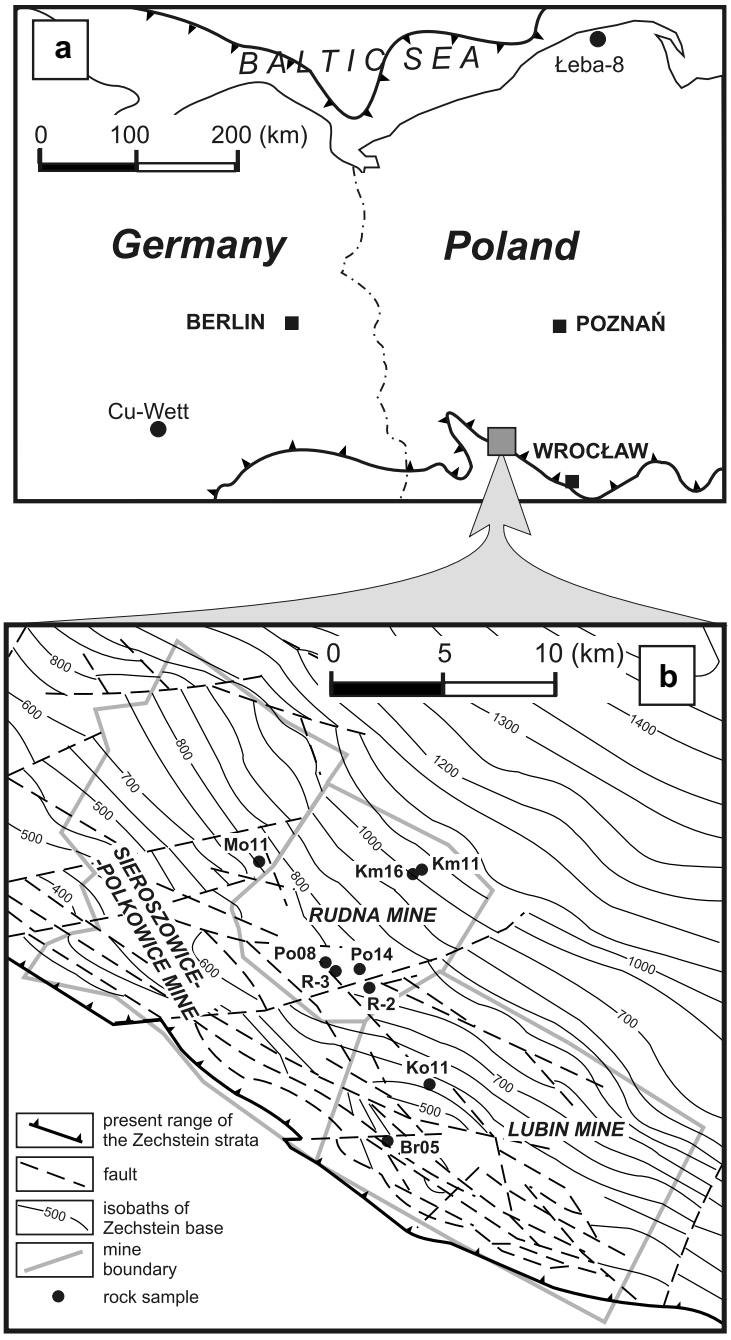

Fig. 1. (a) Index map of the study area with locations of sample sites. Extent of the Zechstein strata is after Peryt (1989). (b) Structure map of base of Zechstein strata, with location of Kupferschiefer sample sites in southwestern Poland. Isobaths and faults are after Downorowicz (1996).

2.3. Product analyses

Molecular compositions of the generated gases (C_1 to C_6 hydrocarbons, CO, CO_2, N_2, H_2S, $O_2 + Ar$, He, and H_2) in mole % were determined on a Hewlett–Packard 6890 gas chromatograph configured by Wasson · Ece Instruments with two thermal conductivity detectors and one flame ionization detector. The determined mole percentages were converted into moles and mass quantities based on the ideal-gas law and recorded collection pressures, temperatures, and volumes. The analyses were checked by calculating the moles of helium recovered at the end of the experiment with the known moles of helium introduced at the beginning of the experiments. The comparison gave acceptable results with the mean difference between the initial and final moles of helium of $-2.6 \pm 1.6\%$ of initial quantities between 34.2 and 39.0 mmol. The negative difference is attributed to neglecting the solubility of helium in

Table 1
Description of Kupferschiefer sample locations

Sample No.	Mine disrict	Mine name	Shaft/level	Depth (m)	Province	Country
Br05	Lubin-Sieroszowice	Lubin	L-1/610	351.8	Lower Silesia	Poland
Cu-Wett	Mansfeld	Wettin	Wettin	162.0	Sachsen-Anhalt	Germany
Km11	Lubin-Sieroszowice	Rudna	R-7/1100	1053.7	Lower Silesia	Poland
Km16	Lubin-Sieroszowice	Rudna	R-7/1100	1030.3	Lower Silesia	Poland
Ko11	Lubin-Sieroszowice	Lubin	L-1/610	578.1	Lower Silesia	Poland
Łeba-8	NA	NA	NA	707.9	Eastern Pomerania	Poland
Mo11	Lubin-Sieroszowice	Sieroszowice	SW-1/1000	984.9	Lower Silesia	Poland
Po08	Lubin-Sieroszowice	Rudna	R-2/1000	807.2	Lower Silesia	Poland
Po14	Lubin-Sieroszowice	Rudna	R-2/1000	839.3	Lower Silesia	Poland
R-2a	Lubin-Sieroszowice	Rudna	R-2/1000	953.9	Lower Silesia	Poland
R-2d	Lubin-Sieroszowice	Rudna	R-2/1000	953.7	Lower Silesia	Poland
R-3	Lubin-Sieroszowice	Rudna	R-2/1000	1017	Lower Silesia	Poland

NA, not applicable because sample is from a well core.

the expelled immiscible oil, water, and rock bitumen in the final recovered He calculation.

Leco TOC and Rock Eval analyses were conducted on the original unheated rocks and recovered rocks with a Leco CR-12 carbon analyzer and Delsi Model II instrument, respectively. The kerogen was isolated from the rocks by sequential acid digestion involving dilute HCl, 49% HF, and concentrated HCl, with a final heavy liquid (zinc bromide) separation and a Soxhlet extraction with an azeotrope of dichloromethane:methanol (93:7 w/w). Elemental analyses (i.e., C, H, N, S, and O) were determined on a Carlo Erba EA1108 instrument using sulfanilamide as a standard for carbon, hydrogen, nitrogen, and total sulfur and acetanilide as a standard for oxygen. Chemical analyses on the original and recovered rocks were conducted by ICP-OES for major oxides (SiO_2, Al_2O_3, Fe_2O_3, FeO, MnO, CaO, Na_2O, K_2O, TiO_2, and P_2O_3), and ICP-MS for trace elements (Ag, Cr, Co, Ba, Be, Bi, Cd, Cu, Mo, Ni, Pb, Rb, Sr, V, W, Zn, and Zr) and rare earth elements (Ce, Cs, Eu, Hf, La, Lu, Nd, Sc, Sm, Tb, Th, U, Y, and Yb). Fire assay-ICP/MS was used for determing of Pd, Pt, and Au. Hg was determined by cold-vapor FIMS. Loss on ignition (LOI) was determined gravimetrically. Total sulfur was analyzed with a Leco SC-132 sulfur analyzer and Polish Standard PN-90/G-04514.16.

Metallic ore minerals were identified in polished sections of the samples under reflected light using an Axioplan Opton microscope. In addition to this petrographic examination for native copper, the samples were analyzed by X-ray diffraction using a PANalytic X Perto Pro X-ray diffractometer with Cu-Kα radiation. Sixty-minute scans from 5° to 65° 2θ were run on spun random powder packed mounds with special attention to the (1 1 1) peak for native copper at a *d*- spacing of 2.087 Å. The samples were pretreated with 6 N HCl for 1 h to remove calcite, which has a (2 0 0) peak at 2.096 Å that could potentially interfere with the main native copper peak. Standards of micronized quartz and 3-μm dendritic copper indicated that concentrations of native copper as low as 0.5 wt% were detectable.

Stable carbon isotopes ($\delta^{13}C$ vs. V-PDB) were measured on methane, ethane, propane, butanes, and carbon dioxide with a Hewlett–Packard gas chromatograph interfaced with a Micromass Optima continuous-flow isotope ratio mass spectrometer (IRMS). $\delta^{13}C$ of the isolated kerogens were measured on a Finnigan Delta Plus. Analytical precision for $\delta^{13}C$ values is estimated to be $\pm 0.2‰$. Hydrogen isotopes (δD vs. V-SMOW) of the methane and waters were measured on a Finnigan Delta Plus, with an analytical precision estimated to be $\pm 3‰$.

3. RESULTS

3.1. Original Unheated Samples

The major oxides and ore elements (Cu, Pb, and Zn) of the Kupferschiefer samples are given in Table 2. An overall description of the inorganic fraction of these shales can be depicted on a ternary diagram of SiO_2, Al_2O_3, and CO_2 (carbonate), as shown in Fig. 2. Inorganic CO_2 is directly related to carbonate mineral content, and Al_2O_3 can be used as a general proxy for the clay-mineral content (e.g., Cubitt, 1979, p. 70). Fig. 2 shows that all of the samples have a similar proportionality of SiO_2 to Al_2O_3 (i.e., 3:1), with CO_2 content showing the greatest differences among the samples. The similar SiO_2:Al_2O_3 ratios indicate that the quartz to clay mineral contents are similar and are within the range of mean SiO_2:Al_2O_3 ratios published for other shales (Fig. 2). Illite is reported to be the main clay mineral (Pieczonka et al., 2001), and this is supported by a good positive correlation between K_2O and Al_2O_3 (Fig. 3a). The samples show a continuum in inorganic CO_2 from less than 1 wt% to nearly 24 wt% (Table 2). This varying carbonate content is in agreement with the lithologic description of Kupferscheifer as shale or marlstone (Jowett et al., 1991). Calcite and dolomite are reported to be the main carbonate minerals (Pieczonka et al., 2001), and this is supported by a good positive correlation between inorganic CO_2 and the sum of CaO and MgO (Fig. 3b).

All of the samples are organic rich with TOC values ranging from 3.9 to 14.6 wt% (Table 2), which is within the range of 1–17 wt% previously reported for the mineralized Polish Kupferschiefer (Sawłowicz, 1993). The organic matter is predominantly of Type-II alginite kerogen and is indigenous to the rocks (Sawłowicz et al., 2000). This later conclusion is supported by the bivariate plot in Fig. 4a, which shows two positive correlation trends between Al_2O_3

Table 2
Major oxides, carbon species, sulfur species, ore metals (Cu, Pb, Zn), and trace[a] elements (Table 3) of original unheated rocks (wt%)

Sample	Br05	Cu-Wett	Km11	Km16	Ko11	Łeba-8	Mo11	Po08	Po14	R-2a	R-2d	R-3
SiO_2	31.80	24.20	26.14	29.84	24.94	21.46	33.42	36.08	32.68	34.67	25.69	31.14
Al_2O_3	13.04	7.83	9.03	10.02	8.94	5.86	12.06	12.49	11.87	13.26	9.20	11.24
Fe_2O_3	0.01	1.66	3.12	2.11	1.98	1.31	0.14	2.07	2.97	2.66	1.79	2.02
FeO	2.24	1.16	0.95	1.51	0.71	1.33	1.26	0.69	0.44	0.71	1.25	0.71
MnO	0.05	0.29	0.15	0.16	0.20	0.13	0.14	0.03	0.12	0.03	0.24	0.09
MgO	1.93	1.41	3.10	2.79	7.61	4.13	2.88	1.35	3.20	1.60	2.37	2.74
CaO	1.67	17.36	5.01	4.91	13.03	25.64	5.28	1.50	5.03	2.17	12.89	6.19
Na_2O	0.09	0.06	0.43	0.83	0.29	0.54	0.54	0.40	0.57	0.28	0.32	0.39
K_2O	3.23	1.89	2.47	2.79	2.52	1.88	3.41	3.62	3.50	3.84	2.63	3.37
TiO_2	0.59	0.39	0.45	0.47	0.39	0.32	0.57	0.60	0.51	0.62	0.40	0.49
P_2O_5	0.15	0.31	0.17	0.13	0.11	0.07	0.12	0.15	0.21	0.41	0.12	0.10
CO_2	0.7	12.8	7.0	5.5	17.6	23.8	5.1	1.1	5.9	0.7	11.0	6.6
TOC[b]	11.90	12.30	12.20	13.40	7.00	3.90	9.60	11.40	10.30	14.60	9.00	8.80
S (total)	4.60	3.63	6.41	5.16	2.90	1.89	3.78	5.51	4.55	6.36	4.12	4.53
Cu	17.95	0.18	2.55	6.45	1.20	0.03	8.87	9.01	6.87	8.69	2.66	5.23
Pb	0.02	1.46	4.65	0.72	3.05	0.02	0.13	0.80	0.18	0.35	4.06	3.32
Zn	0.01	3.66	1.13	0.44	1.25	0.02	0.01	0.00	0.00	0.00	0.12	0.94
Trace[a]	0.73	0.71	0.50	1.03	0.64	0.14	0.42	2.74	0.51	0.68	0.29	0.37
LOI	19.47	26.36	25.60	27.41	23.93	24.74	21.28	20.31	25.18	22.73	20.96	21.36
Total	92.97	88.93	85.45	91.61	90.78	87.62	90.52	91.84	93.84	92.72	85.00	89.70

[a] Trace element from Table 5 excluding Cu, Pb, and Zn.
[b] Total organic carbon (LECO).

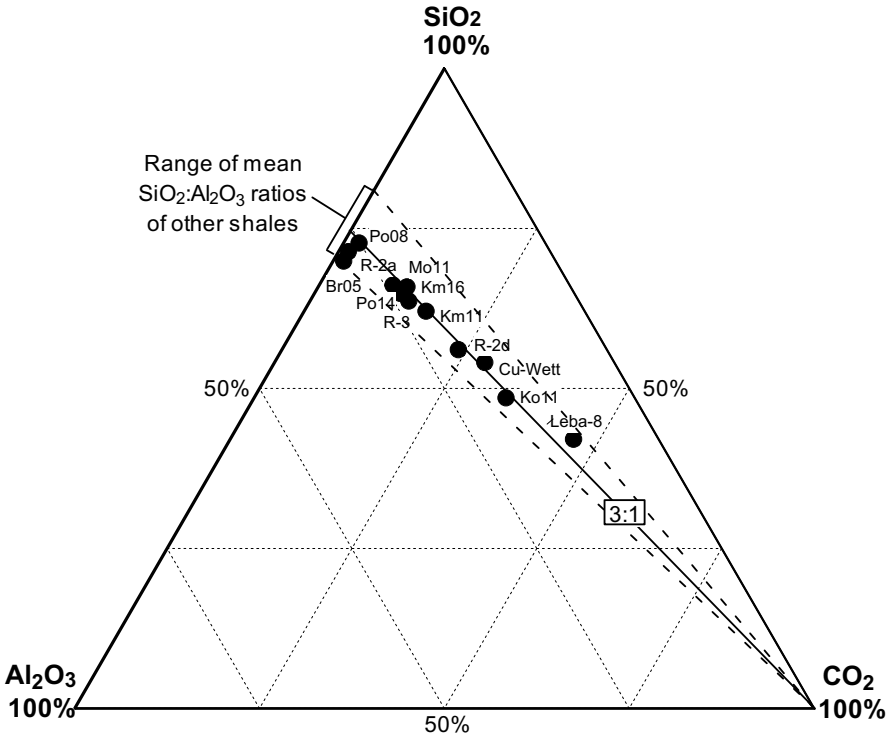

Fig. 2. SiO_2–Al_2O_3–CO_2 (carbonate) ternary diagram of Kupferschiefer samples. Solid tie line shows average SiO_2:Al_2O_3 ratio (3:1) of samples with varying CO_2 (carbonate) content. Dashed tie lines show upper and lower limits of the SiO_2:Al_2O_3 ratios. Bracket showing range of mean SiO_2:Al_2O_3 ratios for other shales is based on mean values calculated from chemical analyses reported by Clarke (1924), Keith and Degens (1959), Turekian and Wedepohl (1961), Cubitt (1979), Chen and Shaffer (1979), Pearson (1979), Gromet et al. (1984), Cullers (1994) and Rimmer (2004).

and TOC contents of the samples. Using Al_2O_3 as a proxy for clay-mineral content, a distal low-energy water column would favor the deposition of fine clay minerals and the degraded remains of plankton. These positive correlations

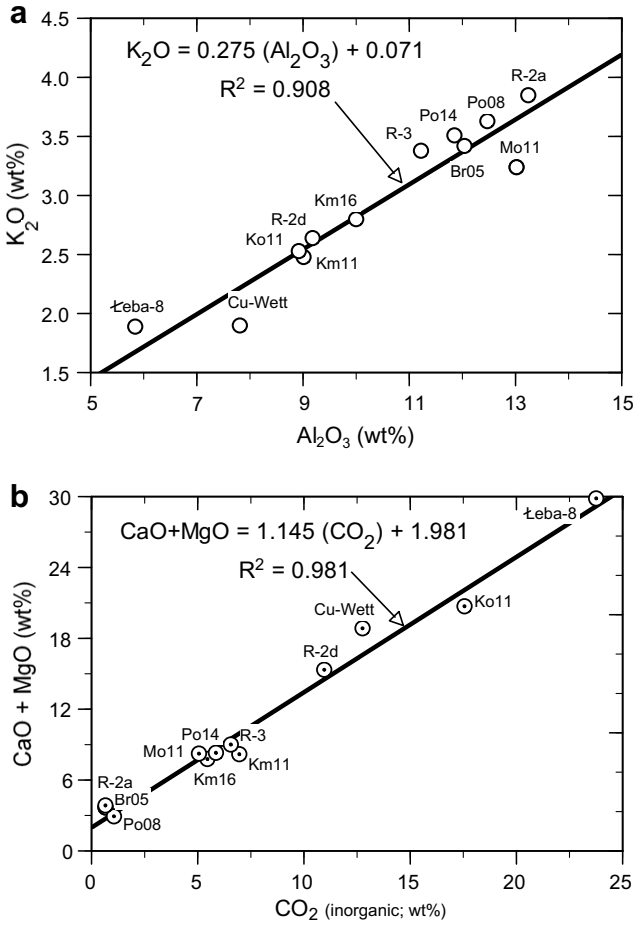

Fig. 3. Bivariate plots of (a) K_2O versus Al_2O_3 and (b) sum of MgO and CaO versus CO_2 (carbonate). Linear-regression correlation coefficients are designated as *R*.

may also be explained by clay minerals playing an important role in the accumulation and preservation of sedimentary organic matter of black shales as proposed by Kennedy et al. (2002). The two different trends may be the result of different depositional settings with one having a higher input or preservation of organic matter than the other. These trends may also be the result of dilution by carbonate minerals. Fig. 4b shows two negative correlation trends between TOC and carbonate CO_2 that are defined by the same samples that define the two positive trends with Al_2O_3 (Fig. 4a). Therefore, the observed covariance of Al_2O_3 and TOC may be a result of dilution by addition of carbonate minerals during deposition, diagenesis, or mineralization.

Total sulfur gives the best single-trend correlation with TOC, as shown in Fig. 4c. With the exception of sample Cu-Wett, the samples plot between the normal marine and euxinic trends reported by Berner (1984) and Leventhal (1983), respectively. Forcing the regression line through the origin gives an average TOC/sulfur ratio of 2.3 (Fig. 4c), which is within the range of values reported for the German Kupferschiefer by Bechtel et al. (2001). TOC/sulfur ratios between normal marine and euxinic values indicate that the sulfur in the mineralized section is indigenous and not introduced by the ore-forming fluid. This interpretation is in general agreement with previous interpretations (e.g., Sun and Puttmann, 1997; Bechtel et al., 2001).

Copper, lead, and zinc are the most abundant ore metals in the Kupferschiefer and average 10.48, 0.41, and 0.08 wt% of the rock, respectively (Pieczonka et al., 2001). Compared to the Cu, Pb, and Zn concentrations in an average shale (i.e., 57, 20, and 80 ppm, respectively; Krauskopf, 1967, Appendix III), these samples on the average are enriched by factors of 1839, 205, and 10, respectively. Their concentrations are given in Table 2, and their proportionality to one another is shown in Fig. 5. Seven of the samples (Br05, Kn16, Mo11, Po08, Po14, R-2a, and R-3) have Cu contents between 5 and 18 wt% (Table 2), which constitutes more than 50% of the three major ore metals (Fig. 5). Samples Km11, Ko11, and R-2d have the highest Pb concentrations between 3 and 5 wt% (Table 2), which account for more than 50% of three major ore metals (Fig. 5). Sample Cu-Wett from Germany was included in the study because of its high Zn concentration of 3.66 wt% (Table 2), which accounts for more than 50% of the three major ore metals (Fig. 5). The Łeba-8 sample is from outside the mineralized ore district and contains less than 0.04 wt% of all three metals (Table 2) in near equal proportions (Fig. 5). TOC and

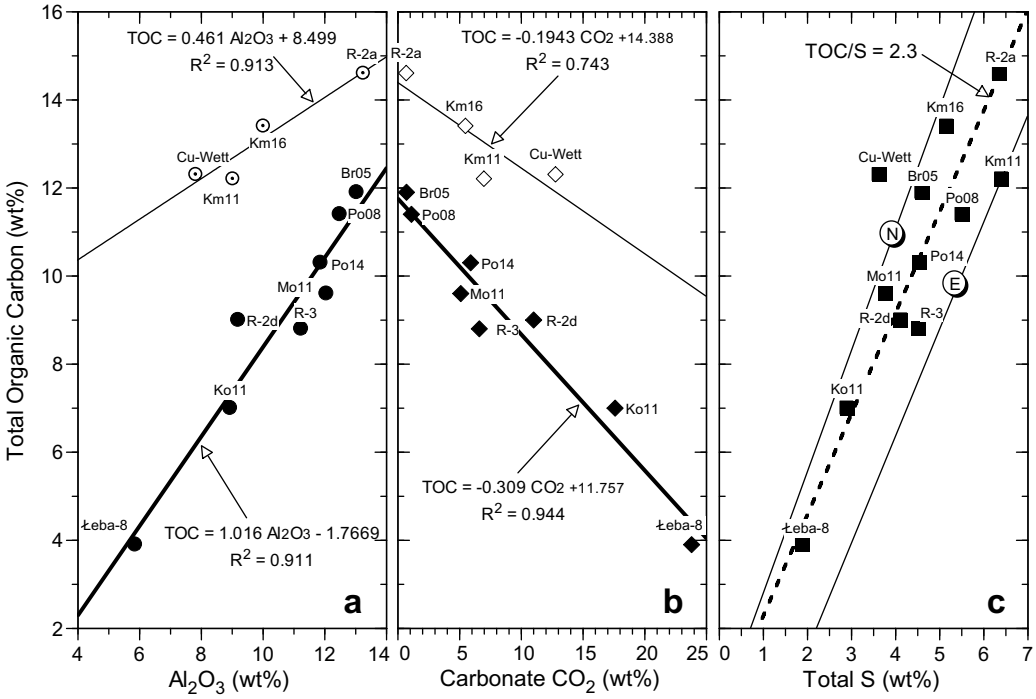

Fig. 4. Bivariate plots of total organic carbon (TOC) versus (a) Al_2O_3, (b) carbonate CO_2, and (c) total sulfur. Linear-regression correlation coefficients are designated as *R*. The line labeled with encircled N is for normal marine sediments as defined by Berner (1984), and the line labeled with encircled *E* is for Black Sea euxinic sediments as defined by Leventhal (1983).

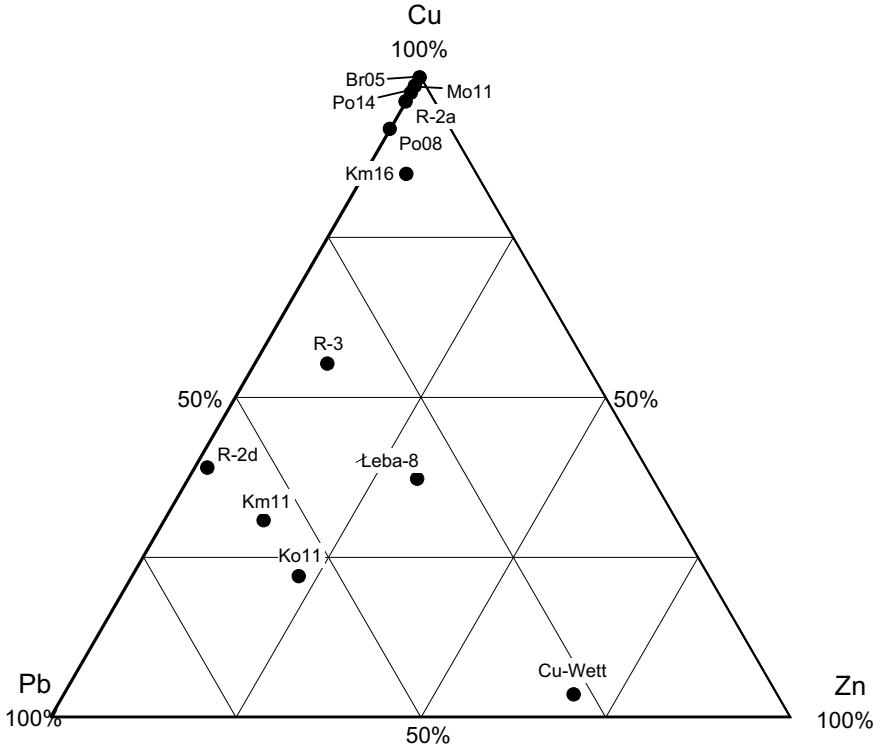

Fig. 5. Cu–Pb–Zn ternary diagram of Kupferschiefer samples based on normalized weight percent.

total sulfur contents showed no significant correlations with these metals or their summation. This lack of correlation indicates that the amount and type of major metals in the samples were controlled by the chemistry (i.e., metal

activity, Eh, pH, and chlorinity), temperature, and source of the mineralizing fluids, which is in general agreement with interpretations of Jung and Knitzschke (1976) and Mayer and Piestrzyński (1985).

The ore minerals identified in the samples are presented in Table 3. Chalcocite (Cu_2S) and covellite (CuS) are the main copper sulfide minerals, with the former being the most common and abundant. Iron–copper sulfides include bornite (Cu_5FeS_4) and chalcopyrite ($CuFeS_2$) with the former being the most prevalent. Pyrite (FeS_2) is present in all but three samples (Km11, Mo11, and R2d) and is the major sulfide in the immature Łeba-8 sample. Except for sample Mo11, galena (PbS) and sphalerite (ZnS) always occur in the same samples but in varying proportions. All of the samples have two or more ore minerals that occur in major or moderate abundances with the exception of sample Mo11, which contains only a major abundance of chalcocite (Cu_2S). This mineral is one of the most sulfur-deficient copper sulfides, which is sometimes associated with native copper (Bastin, 1933). Petrographic examination and X-ray diffraction analysis of this sample, as well as the other samples showed no detectable native copper (Cu^o) within the detection limits of ~2 μm and 0.5 wt%, respectively. However, petrographic examination revealed minor or trace abundances of native silver (Ag^o) in three of the samples (Po08, Po14, and R-2a; Table 3).

Organic matter in the original unheated samples is characterized by the geochemical parameters given in Table 4. The kerogen atomic H/C ratio, vitrinite reflectance (%R_r), Rock Eval T_{max}, and bitumen/TOC ratio indicate that the samples are thermally immature to marginally mature, which is in agreement with Püttmann et al. (1991). Although all of the mentioned thermal maturity parameters are in general agreement, the kerogen atomic H/C ratio was

Table 3
Ore minerals identified in original samples with intra-sample nominal abundances: major (+++); moderate (++); minor (+); trace (tr); and not observed (-)

Mineral	Br05	Cu-Wett	Km11	Km16	Ko11	Łeba-8	Mo11	Po08	Po14	R-2a	R-2d	R-3
Native Copper (Cu^o)	–	–	–	–	–	–	–	–	–	–	–	–
Chalcocite (Cu_2S)	+++	–	–	++	–	–	+++	++	+	+++	+	–
Covellite (CuS)	+	–	–	+	–	–	–	Tr	–	–	–	–
Bornite (Cu_5FeS_4)	+++	–	–	+++	–	–	–	+++	+++	++	+++	+
Chalcopyrite ($CuFeS_2$)	+	+	++	–	++	–	–	++	++	–	+++	++
Pyrite (FeS_2)	Tr	+		+	+	+++	–	+	+	+	–	+
Sphalerite (ZnS)	–	+++	+++	+	+++	++	–	–	–	+	+	+++
Galena (PbS)	–	++	++	++	++	+	+	tr	–	++	+++	+
Native Silver (Ag^o)	–	–	–	–	–	–	–	Tr	+	+	–	–

Table 4
Organic geochemical parameters characterizing the organic matter in the original unheated rocks

Sample	Br05	Cu-Wett	Km11	Km16	Ko11	Łeba-8	Mo11	Po08	Po14	R-2a	R-2d	R-3
Leco TOC (wt%)	11.9	12.3	12.2	13.4	7	3.9	9.6	11.4	10.3	14.6	9	8.8
Bitumen (mg/g TOC)	41	36	65	73	62	84	58	63	59	66	68	61
Rock eval indices												
S1 (mg/g rock)	0.83	1.35	3.1	3.4	1.48	0.66	1.34	1.65	1.27	4	1.5	1.62
S2 (mg/g rock)	40.2	35.3	40.6	36.9	28.9	13.2	27.8	44.7	31	56.6	40	29.1
S3 (mg/g rock)	0.81	1.32	0.66	1.99	0.37	2.59	2.12	0.72	2.53	0.72	0.95	1.9
HI (mg/g TOC)	338	287	333	275	413	338	290	392	301	388	444	331
OI (mg/g TOC)	7	11	5	15	5	66	22	6	25	5	11	22
PI (S1/[S1 + S2])	0.02	0.04	0.07	0.08	0.05	0.05	0.05	0.04	0.04	0.07	0.04	0.05
T_{max} (°C)	433	438	435	432	439	419	434	431	431	432	433	432
Kerogen												
$\delta^{13}C$ (‰ vs. V-PDB)	−27.4	−26.9	−27.3	−27.5	−27.3	−27.2	−27.5	−27.2	−27.5	−27.6	−27.1	−27.6
Elemental (wt%)												
Carbon	80.38	85.35	83.34	85.32	86.19	71.34	80.45	80.18	81.71	81.90	84.39	82.09
Hydrogen	6.53	6.14	6.23	7.03	7.17	7.51	6.31	6.76	7.26	6.73	7.15	6.83
Oxygen	4.45	3.71	4.08	4.32	2.69	13.05	4.41	3.68	4.87	4.18	3.08	4.89
Nitrogen	2.31	2.47	2.28	2.29	2.11	2.52	2.48	2.40	2.26	2.42	2.35	2.41
Total Sulfur	6.33	2.32	4.06	1.03	1.84	5.57	6.36	6.98	3.90	4.77	3.02	3.78
Atomic ratio												
H/C	0.97	0.86	0.89	0.98	0.99	1.25	0.93	1.00	1.06	0.98	1.01	0.99
O/C	0.04	0.03	0.04	0.04	0.02	0.14	0.04	0.03	0.04	0.04	0.03	0.04
N/C	0.025	0.025	0.023	0.023	0.021	0.030	0.026	0.026	0.024	0.025	0.024	0.025
%Vitrinite R_r	0.88	0.94	0.89	0.87	0.86	0.66	0.98	0.91	0.91	0.87	0.85	0.88

used as the discriminating parameter for thermal maturation because of its greater sensitivity to stages of petroleum generation (Lewan, 1985; Baskin, 1997). Atomic H/C and O/C ratios of the isolated kerogens are plotted on a van Krevelen diagram modified after Hunt (1996) in Fig. 6. The Łeba-8 sample from the unmineralized Kupferschiefer is the most immature with an atomic H/C ratio of 1.25 and a vitrinite reflectance of 0.66 $\%R_r$ (Table 4). The other samples are marginally mature with a mean atomic H/C ratio of 0.97 ± 0.06, with sample Po14 being slightly less mature and samples Mo11, Km11, and Cu-Wett being slightly more mature. Despite their marginal and small variations in thermal maturity, the kerogen in all of the samples is best classified as Type II (Fig. 6). A similar precursor for these kerogens is indicated by their similar $\delta^{13}C$ values ($-27.3 \pm 0.2‰$; Table 4), which is a parameter that does not change significantly with thermal maturation (Lewan, 1983). If the Łeba-8 sample represents the immature kerogen of the other marginally mature Kupferschiefer samples, the total Fe content of this unmineralized sample can be used to calculate its organic sulfur content and atomic S_{org}/C. This calculation assumes all the Fe occurs as FeS_2 and yields an atomic S_{org}/C of 0.034, which is indicative of a Type-II kerogen and not a high-sulfur Type-IIS kerogen (atomic $S_{org}/C > 0.040$; Orr and Sinninghe Damsté, 1990).

Trace element concentrations in the original unheated samples are given in Table 5. These concentrations are compared in Fig. 7 with those of average shale as defined by Krauskopf (1967, Appendix III). The comparison is divided into transition metals (Fig. 7a) and other trace elements (Fig. 7b). The enriched trace transition metals include Ag, Cd, Hg, Mo, Co, Ni, Cr, and V. With the exception of Cd and Hg, these metals are the least or not enriched in the unmineralized Łeba-8 sample (open circles in Fig. 7a). This observation indicates that most of the trace transition metal enrichment is related to the ore mineralization. U and As are the only other trace elements that show a consistent enrichment greater than one order of magnitude relative to the average shale (Fig. 7b).

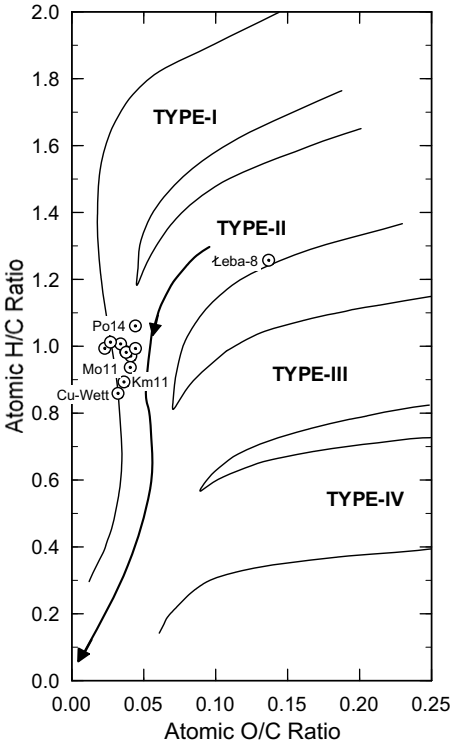

Fig. 6. van Krevelen diagram modified after Hunt (1996) showing the atomic H/C versus O/C ratios of the original unheated Kupferschiefer samples. Arrow depicts increasing thermal maturity for Type-II kerogen.

Evaluating the catalytic potential of the enriched trace- and major-ore transition metals requires their concentrations to be considered in proportion to the TOC in the rock. The rationale is that samples with high metal concentrations and low TOC values should show a greater catalytic effect on gas generation than samples with low metal concentrations and high TOC values. Table 6 gives the transition metal concentrations relative to TOC and these values (mg/g TOC) are used to evaluate their catalytic potential in gas generated by hydrous pyrolysis. Although Pb is not a transition metal, it has been included because of its high concentrations in these samples and its reported catalytic activity in ethene hydrogenation (Masel, 2001, Fig. 14.24). Ratios of maximum to minimum values of the metals given in Table 6 show that Zn has the greatest range of more than three orders of magnitude (Max/Min = 1417) and Mo has the smallest range of a factor of two. Cu is the most abundant of the metals on a TOC basis and has a range of more than two orders of magnitude (Table 6). With the exception of Cr and Cd, the Łeba-8 sample, which was not mineralized, contains the lowest metal content on a TOC basis.

3.2. Experimental results

Tables 7 and 8 give the organic geochemical parameters of the rock recovered from the hydrous pyrolysis experiments at 330 and 355 °C after 72 h, respectively. Excluding the immature Łeba-8 sample, the mean vitrinite reflectance increased from 0.89 $\%R_r$ for the original unheated samples to 1.04 $\%R_r$ after 330 °C for 72 h and 1.61 $\%R_r$ after 355 °C for 72 h. The maturity changes from the original sample to the recovered samples heated at 330 and 355 °C are also indicated by the mean atomic H/C ratio (0.97 to 0.74 and 0.62, respectively), the mean Rock Eval hydrogen index (345 to 233 and 93 mg/g TOC, respectively), and Rock Eval T_{max} (434 to 441 and 455 °C, respectively). Although the original unheated Łeba-8 sample was immature, its vitrinite reflectance (0.95$\%R_r$), atomic H/C ratio (0.74), and T_{max} (444 °C) after 330 °C for 72 h indicate that its increase in maturity is comparable to maturities attained by the other samples. Its vitrinite reflectance (1.52$\%R_r$), atomic H/C ratio (0.70), and T_{max} (449 °C) after 355 °C for 72 h indicate that the increase in maturity is only slightly less than but comparable to that attained by the other samples. This observation is in general agreement with the hydrous pyrolysis study of different ranked coals (0.28–1.11 $\%R_r$) attaining similar maturity levels (1.50–1.85 $\%R_r$) after heating at 360 °C for 72 h (Kotarba and Lewan, 2004).

Table 5
Trace transition metals and other trace elements in ppm of original rock except those noted otherwise with an * for ppb

Element	Br05	Cu-Wett	Km11	Km16	Ko11	Łeba-8	Mo11	Po08	Po14	R-2a	R-2d	R-3	Avg. Shale[a]
Transition metals													
Sc	11.5	8.2	10.0	10.9	11.9	6.2	12.3	13.6	12.8	14.3	9.2	12.2	10.0
V	1850	1436	1512	1443	925	268	1805	1357	1444	2099	997	1368	130.0
Cr	310.0	148.0	212.0	227.0	250.0	96.0	282.0	267.8	233.3	325.4	149.6	297.1	100.0
Co	844	97	576	430	1800	16	214	593	660	955	140	119	20.0
Ni	550.4	321.6	452.5	381.5	199.3	69.0	382.1	570.1	491.9	550.8	274.4	414.2	95.0
Zr	102	91	114	172	70	74	128	154	120	127	121	178	200.0
Mo	480	530	470	520	300	100	300	390	440	800	350	270	2.0
Ag	292.7	47.1	80.9	197.0	78.6	1.3	151.1	267.4	263.5	251.7	233.8	175.3	0.1
Cd	6.1	169.6	46.1	21.8	35.2	3.6	3.4	2.4	3.6	3.4	5.8	31.6	0.3
La	33.0	40.1	31.1	27.9	31.7	23.4	34.1	30.2	31.8	38.1	25.0	27.5	40.0
Hf	5.8	4.3	3.5	7.7	4.5	2.4	5.3	7.0	4.7	5.4	3.5	5.2	6.0
Ta	<1	<1	<1	<1	<1	<1	1.0	<1	<1	1.5	<1	1.5	ND
W	<3	<3	<3	<3	<3	<3	<3	<3	<3	<3	<3	<3	2.0
Pd*	<4	<4	<4	<4	<4	12.4	<4	<4	<4	<4	<4	<4	<50
Ir*	<5	<5	<5	<5	<5	<5	<5	<5	<5	<5	<5	<5	<50
Pt*	<5	<5	<5	<5	<5	<5	<5	<5	<5	<5	<5	<5	<50
Au*	8.0	7.7	6.8	11.1	3.7	5.6	7.5	5.1	7.7	7.8	5.7	9.0	<50
Hg*	1642	3377	3173	3085	4152	62	589	54266	15072	18104	16664	5715	400.0
Other trace elements													
Se	<3	<3	70	60	46	24	<3	45	72	56	37	50	0.6
Rb	188	106	165	222	204	56	225	195	213	258	160	233	140.0
Sr	728	154	434	4492	114	230	156	15848	102	134	87	107	450.0
Ba	202	3521	332	1621	159	347	213	6864	219	243	159	212	580.0
Cs	44.2	17.7	40.0	46.4	42.6	3.5	74.6	60.7	50.6	56.1	39.6	48.6	5.0
Ce	51.5	64.5	52.0	48.5	50.5	36.5	54.5	50.5	58.5	73.0	44.5	42.5	50.0
Nd	24.0	29.5	25.0	25.5	23.5	14.5	23.5	26.0	34.5	50.5	16.5	15.5	23.0
Sm	4.6	6.7	7.9	4.9	7.3	2.9	5.4	6.1	11.0	16.6	4.9	4.3	5.5
Eu	1.0	1.3	2.0	1.2	0.7	0.6	1.0	0.6	1.7	3.1	1.2	0.9	1.0
Tb	1.6	1.1	1.3	1.5	<0.5	0.5	<0.5	<0.5	1.3	2.4	0.8	<0.5	0.9
Yb	1.0	1.7	1.6	1.7	1.9	1.2	2.0	1.6	1.9	2.4	1.6	1.8	3.0
Lu	0.1	0.3	0.3	0.3	0.3	0.2	0.3	0.3	0.3	0.4	0.3	0.3	0.7
As	1431.1	177.8	346.7	264.9	2000.0	14.2	136.9	530.7	521.8	698.7	40.9	29.3	6.6
Sb	9.8	12.4	9.9	7.1	7.0	1.7	4.2	7.2	8.6	11.0	3.9	4.0	1.5
Th	9.6	7.2	7.3	7.9	8.4	4.8	9.1	9.5	8.7	9.7	6.2	9.2	11.0
U	73.8	119.5	28.9	23.3	21.0	11.6	23.1	25.6	27.3	37.3	17.3	16.1	3.2
TOTAL	7257	7117	5035	10270	6396	1409	4247	27378	5053	6842	2946	3680	1888

[a] Average shale from compilation by Krauskopf (1967, Appendix III).

The increase in mean bitumen content of all the samples from 61 to 282 mg/g TOC after 330 °C for 72 h is in agreement with previously reported values indicative of kerogen decomposition to bitumen (Lewan, 1985). The decrease in mean bitumen content from 282 mg/g TOC after heating at 330 °C for 72 h to 151 mg/g TOC after heating at 355 °C for 72 h is in agreement with previously reported values indicative of bitumen decomposition to immiscible oil (Lewan, 1985). At these experimental conditions, a petrographic study has shown that the entire matrix and microporosity of a source rock is impregnated with the generated bitumen as a result of the volume increase associated with kerogen decomposition to bitumen (Lewan, 1987). The pervasiveness of this process is realized by reports of bitumen impregnating the interlayers of expandable clay-minerals in source rocks (Lewan and Whitney, 1993; Cai et al., 2008). This suggests maximum possible contact between the generated bitumen and metals within the rocks, with no liquid water films or pore fillings to minimize contacts between metals and organic matter.

The amounts and types of gases generated at 330 °C and 355 °C after 72 h are given on a TOC basis (i.e., mg/g TOC) in Tables 9 and 10, respectively. Under these conditions, the 330 °C experiments represents early gases that are generated during the final stages of bitumen generation from kerogen decomposition, and the 355 °C experiments represent later gases that are generated during oil generation from bitumen generation (Lewan, 1985). Thermal cracking of immiscible oil to gas is not likely at 355 °C for 72 h because previous studies show this reaction in hydrous pyrolysis experiments requires temperatures in excess of 365 °C for 72 h (Ruble et al., 2003, Fig. 3; Lewan et al., 2006, Fig. 5). Generated non-hydrocarbon gases from both experimental conditions include molecular hydrogen, hydrogen sulfide, carbon dioxide, and trace amounts of carbon monoxide. The observed variations in non-hydrocar-

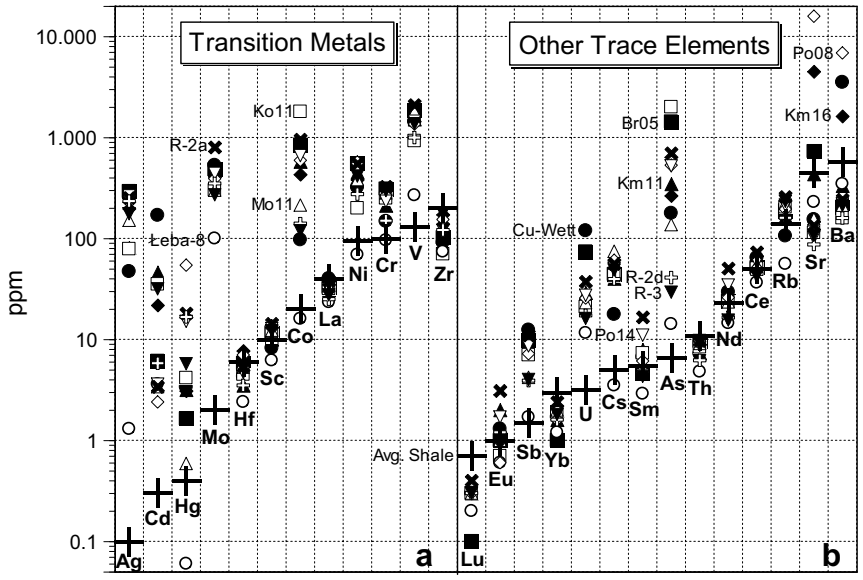

Fig. 7. Plot comparing concentration of trace elements in original unheated Kupferschiefer samples with average shale as defined by Krauskopf (1967, Appendix III): (a) transition metals and (b) other trace metals. Sample designations are given to the left of representative symbols (Br05, solid squares; CuWett, solid circle; Km11, solid upward triangle; Km16, solid diamond; Ko11, open square; Łeba-8, open circle; Mo11, open upward triangle; Po08, open diamond; Po14, open downward triangle; R-2a, solid x; R-2d, open cross; R-3, solid downward triangle; and average shale, solid cross).

Table 6
Transition metal concentrations relative to total organic carbon (mg/g TOC) in original samples

Sample	Cu	Pb	Zn	V	Co	Mo	Ni	Cr	Ag	Cd	Hg
Br05	1508.40	1.82	0.59	15.55	7.09	4.03	4.63	2.61	2.46	0.05	0.014
Cu-Wett	14.84	118.40	297.58	11.67	0.79	4.31	2.61	1.20	0.38	1.38	0.027
Km11	209.34	381.23	92.55	12.39	4.72	3.85	3.71	1.74	0.66	0.38	0.026
Km16	481.69	53.82	32.84	10.77	3.21	3.88	2.85	1.69	1.47	0.16	0.023
Ko11	172.09	435.18	178.02	13.21	25.71	4.29	2.85	3.57	1.12	0.50	0.059
Łeba-8	6.79	5.82	5.68	6.87	0.41	2.56	1.77	2.46	0.03	0.09	0.002
Mo11	923.60	13.24	0.77	18.80	2.23	3.13	3.98	2.94	1.57	0.04	0.006
Po08	790.42	70.42	0.30	11.90	5.20	3.42	5.00	2.35	2.35	0.02	0.476
Po14	667.16	17.07	0.45	14.02	6.41	4.27	4.78	2.27	2.56	0.03	0.146
R-2a	595.19	24.14	0.21	14.38	6.54	5.48	3.77	2.23	1.72	0.02	0.124
R-2d	295.82	451.29	13.82	11.08	1.56	3.89	3.05	1.66	2.60	0.06	0.185
R-3	594.70	377.10	107.14	15.55	1.35	3.07	4.71	3.38	1.99	0.36	0.065
Mean	522	162	60.8	13.0	5.44	3.85	3.64	2.34	1.58	0.26	0.096
Max/Min[a]	222	248	1417	3	63	2	3	3	87	69	238

[a] Maximum valule divided by minimum value.

bon gases among the samples have no significant correlations with the metals given in Table 6. The immature Łeba-8 sample generated the most H_2S and CO_2 under both experimental conditions (Tables 9 and 10). Excluding this immature sample, the mean H_2S and CO_2 contents increased from the 330 °C experiments to the 355 °C experiments by 186% and 16%, respectively.

As discussed by Lewan (1997), some of the molecular hydrogen is derived from the water dissolved in the bitumen that impregnates the rock matrix. The oxygen from this reactive water results in generation of high CO_2 contents. Therefore, the variations in the amounts of generated CO_2 gas from the samples (Tables 9 and 10) can be attributed to several sources including decarboxylation of the original kerogen, dissolved water interaction with carbonyl groups, and partial dissolution of carbonate minerals. These multiple sources are evidenced by the wide range of $\delta^{13}C$ values of the CO_2 (−10.4 to 5.2‰, Tables 9 and 10). The exceptionally high CO_2 generated from the Łeba-8 sample is attributed to the immaturity of the kerogen compared to the other samples as shown by its higher atomic O/C ratio in Fig. 6.

The amount of H_2S generated is less than 10 mg/g TOC for all of the samples at both experimental conditions with the exception of the Łeba-8 sample, which generated 24.0 mg/g TOC in the 355 °C experiment (Table 10).

Table 7
Organic geochemical parameters characterizing the organic matter in recovered rock after 330 °C for 72 h

Sample	Br05	Cu-Wett	Km11	Km16	Ko11	Łeba-8	Mo11	Po08	Po14	R-2a	R-2d	R-3
Leco TOC (wt%)	9.0	10.9	10.7	10.0	5.6	2.4	7.9	11.3	8.3	11.5	7.9	8.6
Bitumen (mg/g TOC)	243	105	282	179	312	292	266	384	279	403	371	270
Rock eval indices												
S1 (mg/g rock)	3.4	1.8	4.8	2.4	1.9	1.1	2.6	8.7	3.4	8.8	4.9	3.0
S2 (mg/g rock)	24.9	23.5	25.7	18.2	16.8	3.6	18.8	31.7	21.8	29.5	23.2	21.8
S3 (mg/g rock)	0.4	0.4	0.4	0.7	0.5	0.6	0.7	0.5	0.4	0.4	0.6	0.6
HI (mg/g TOC)	243	199	214	161	297	144	187	260	228	234	281	258
OI (mg/g TOC)	3	4	3	6	8	22	7	4	4	3	8	7
PI (S1/[S1 + S2])	0.121	0.072	0.158	0.117	0.103	0.237	0.122	0.215	0.136	0.230	0.175	0.120
T_{max} (°C)	441	449	441	445	442	444	441	438	440	437	439	441
Kerogen												
$\delta^{13}C$ (‰ vs. V-PDB)	−27.22	−26.69	−27.23	−27.29	−27.06	−26.81	−27.12	−26.96	−27.21	−27.34	−26.69	−27.29
Elemental (wt%)												
Carbon	85.83	88.17	85.61	84.55	82.92	84.00	83.60	84.11	84.26	83.43	85.86	84.55
Hydrogen	5.13	5.28	5.14	5.34	5.96	5.23	4.63	5.04	4.99	5.30	5.61	5.39
Oxygen	0.13	1.96	1.74	2.48	5.29	4.91	2.38	2.76	1.97	3.38	2.25	3.14
Nitrogen	2.53	2.31	2.51	2.38	2.29	3.30	2.87	2.69	2.60	2.84	2.65	2.65
Total Sulfur	6.38	2.27	5.00	5.24	3.54	2.57	6.52	5.40	6.18	5.04	3.63	4.27
Atomic ratio												
H/C	0.71	0.71	0.72	0.75	0.86	0.74	0.66	0.71	0.71	0.76	0.78	0.76
O/C	0.00	0.02	0.02	0.02	0.05	0.04	0.02	0.02	0.02	0.03	0.02	0.03
N/C	0.001	0.019	0.017	0.025	0.055	0.050	0.024	0.028	0.020	0.035	0.022	0.032
%Vitrinite R_r	1.08	1.15	1.04	0.98	0.98	0.95	1.05	0.98	1.02	1.07	1.05	1.06

Table 8
Organic geochemical parameters characterizing the organic matter in recovered rock after 355°C for 72 h

Sample	Br05	Cu-Wett	Km11	Km16	Ko11	Łeba-8	Mo11	Po08	Po14	R-2a	R-2d	R-3
Leco TOC (wt%)	8.9	10.3	7.8	7.8	5.4	2.6	7.5	9.8	7.8	9.8	6.8	7.0
Bitumen (mg/g TOC)	193	110	135	127	167	180	159	171	121	173	153	150
Rock eval indices												
S1 (mg/g rock)	5.2	3.1	2.8	2.6	1.9	1.1	2.6	6.1	2.8	5.9	3.0	2.4
S2 (mg/g rock)	12.6	11.0	5.9	6.2	6.4	1.2	7.9	9.9	6.1	9.2	7.2	5.6
S3 (mg/g rock)	0.4	0.3	0.3	0.6	0.3	0.6	0.7	0.5	0.5	0.7	0.4	0.4
HI (mg/g TOC)	131	99	72	82	143	48	87	89	74	84	96	68
OI (mg/g TOC)	4	3	4	7	6	22	8	4	6	7	5	4
PI (S1/[S1 + S2])	0.291	0.217	0.320	0.293	0.231	0.478	0.247	0.382	0.315	0.393	0.294	0.305
T_{max} (°C)	453	460	453	456	456	449	452	454	457	448	454	458
Kerogen												
$\delta^{13}C$ (‰ vs. V-PDB)	−27.22	−26.71	−27.13	−27.35	−26.48	−26.64	−27.36	−26.98	−27.12	−27.17	−26.6	−27.15
Elemental (wt%)												
Carbon	83.95	89.26	85.65	87.89	81.96	75.95	85.74	86.44	86.22	83.49	86.13	84.57
Hydrogen	3.92	4.33	4.22	4.32	3.84	4.48	4.17	3.96	4.01	3.99	4.16	4.17
Oxygen	2.10	1.91	4.15	1.55	8.58	13.19	1.34	1.92	2.74	3.76	3.14	5.05
Nitrogen	2.60	2.50	2.90	2.67	2.61	3.06	2.95	2.98	2.80	2.74	2.92	2.89
Total Sulfur	7.43	2.00	3.09	3.57	3.00	3.33	5.80	4.70	4.23	6.02	3.65	3.32
Atomic ratio												
H/C	0.56	0.58	0.59	0.59	0.56	0.70	0.58	0.55	0.55	0.57	0.58	0.59
O/C	0.02	0.02	0.04	0.01	0.08	0.13	0.01	0.02	0.02	0.03	0.03	0.04
N/C	0.027	0.024	0.029	0.026	0.027	0.035	0.030	0.030	0.028	0.028	0.029	0.029
%Vitrinite R_r	1.73	1.67	1.63	1.52	1.54	1.52	1.56	1.55	1.64	1.61	1.61	1.61

Similar to the exceptionally high CO_2 generated from this sample, its immaturity is the likely cause of the exceptionally high H_2S generation. Amrani et al. (2005) have shown that 80 wt% of H_2S generation occurs at low thermal maturities (300 °C for 72 h) in hydrous pyrolysis experiments on Type-IIS kerogen in the Ghareb Limestone. Therefore, the other marginally mature samples are likely to have already released most of their labile sulfur as H_2S. Some of this

Table 9
Types, amounts (mg/g TOC), and stable isotopes of gas generated in hydrous pyrolysis experiments at 330 °C/72 h

Samples	Br05	Cu-Wett	Km11	Km16	Ko11	Łeba-8	Mo11	Po08	Po14	R-2a	R-2d	R-3
Components[a]												
Hydrogen	0.37	0.27	0.38	0.20	0.63	0.62	0.45	0.38	0.36	0.32	0.50	0.42
Hyrdogen sulfide	0.15	0.02	0.00	0.00	2.80	12.48	0.00	1.50	0.47	1.50	1.92	0.56
Carbon dioxide	104.68	42.74	124.53	129.68	296.29	561.49	149.12	26.17	179.84	30.68	114.22	169.95
Carbon monoxide	0.01	0.01	0.01	0.00	0.00	0.00	0.00	0.00	0.03	0.00	0.00	0.00
Non-hydrocarbon total	105.21	43.04	124.92	129.88	299.72	574.59	149.57	28.05	180.70	32.50	116.64	170.93
Methane	3.19	2.41	3.49	2.32	3.13	9.09	3.23	5.57	4.03	4.77	4.53	4.24
Ethane	2.32	1.73	2.45	1.93	2.66	7.04	2.06	5.27	2.65	4.42	3.54	2.91
Ethene	0.00	0.02	0.00	0.00	0.00	0.00	0.00	0.00	0.00	0.00	0.00	0.00
Propane	2.62	1.91	2.75	1.79	2.40	5.68	2.59	4.29	3.21	3.38	3.53	3.37
Propene	0.00	0.00	0.00	0.00	0.04	0.00	0.00	0.00	0.00	0.00	0.00	0.00
n-Butane	1.46	1.05	1.47	1.04	1.50	2.96	1.48	2.04	1.69	1.57	1.80	1.84
i-Butane	0.44	0.32	0.47	0.35	0.52	1.38	0.48	0.66	0.56	0.50	0.60	0.56
n-Pentane	0.73	0.55	0.70	0.53	0.77	1.47	0.78	0.87	0.74	0.49	0.81	0.86
i-Pentane	0.33	0.25	0.30	0.23	0.39	0.86	0.28	0.42	0.37	0.25	0.39	0.37
Hydrocarbon total	11.09	8.24	11.63	8.19	11.41	28.48	10.90	19.12	13.25	15.38	15.20	14.15
Dryness ($C_1/[C_1 - C_4]$)	0.318	0.324	0.328	0.312	0.305	0.348	0.328	0.312	0.332	0.326	0.324	0.328
Ethane/propane	0.885	0.906	0.891	1.078	1.108	1.239	0.795	1.228	0.826	1.308	1.003	0.864
$C_3/[C_1 + C_3]$	0.451	0.442	0.441	0.436	0.434	0.385	0.445	0.435	0.443	0.415	0.438	0.443
$C_4/[C_1 + C_4]$	0.373	0.362	0.357	0.375	0.392	0.323	0.378	0.326	0.358	0.303	0.346	0.361
$i/(n + i)$ Butanes	0.232	0.234	0.242	0.252	0.257	0.318	0.245	0.244	0.249	0.242	0.250	0.233
Methane $\delta^{13}C$[b]	−40.9	−39.5	−41.2	−40.0	−41.6	−37.5	−41.4	−40.8	−38.7	−41.3	−40.2	−40.7
Methane δD[c]	n.a.	−264.0	−233.0	−272.0	n.a.	−341.0	−266.0	−331.0	−269.0	−304.0	−312.0	−302.0
Ethane $\delta^{13}C$[a]	−34.4	−33.6	−33.7	−33.8	−34.8	−32.4	−34.4	−33.9	−33.8	−33.4	−33.6	−33.6
Propane $\delta^{13}C$[a]	−32.4	−30.8	−32.2	−32.2	−33.4	−31.6	−32.5	−32.4	−32.8	−31.6	−32.6	−32.5
n-Butane $\delta^{13}C$[a]	−30.4	−28.8	−30.2	−30.3	−31.5	−31.0	−31.4	−30.9	−30.4	−30.1	−30.5	−30.8
i-Butane $\delta^{13}C$[a]	−29.3	−27.9	−29.1	−29.2	−29.5	−29.3	−30.3	−30.3	−29.3	−28.7	−29.7	−29.8
$CO_2\delta^{13}C$[a]	1.6	−9.3	2.8	2.4	5.2	0.1	1.5	−8.5	2.8	−5.8	1.9	2.7

n.a., not analysed.
[a] Butenes, neopentane, cycopentane, hexanes, and heptanes less than 0.005 mg/g TOC.
[b] ‰ versus V-PDB.
[c] ‰ versus SMOW.

early released H_2S may have reacted with the metals introduced by the mineralizing fluids during ore formation.

The generated hydrocarbon gases also show a wide range of yields for the different samples (Tables 9 and 10), and like the non-hydrocarbon gases there are no significant correlations with the transition metals (Table 6). This lack of correlation is exemplified by Cu in Fig. 8. The notably higher yields from the Łeba-8 sample are again attributed to its immaturity relative to the other samples, which are at marginal maturities (Fig. 6). There is a positive correlation between the hydrocarbon-gas yields from the 330 °C experiments (Fig. 9), and those from the 355 °C experiments, with the latter yields being greater by more than a factor of two. Deviations from the regression line in Fig. 9 and the individual gases (Tables 9 and 10) show no significant correlations with the transition metals. A peculiar observation is that propane contents are greater than ethane contents for many of the samples generated after 330 °C for 72 h. Typically, hydrocarbon contents decrease in a gas as their carbon number increases. Deviations from this typical distribution have been reported for gaseous products from catalytic hydrogenolysis of alkanes on different metals (Olah and Molnár, 2003, pp. 655–657). However, no significant correlations were observed between the ethane/propane ratio and transition metal contents, as exemplified in Fig. 10 for Cu. Unlike the 330 °C experiments, propane contents generated in the 355 °C experiments are less than ethane with the exception of two samples (Ko11 and Łeba-8) that have propane contents slightly higher than ethane.

Increasing dryness of the hydrocarbon gases, as measured by the decimal fraction of methane in the hydrocarbon gases (i.e., $C_1/[C_1$ thru $C_4]$), has been advocated as an indicator of gas generation by metal catalysis (Mango, 1994). Dryness showed no systematic changes or correlations with increasing transition metal contents with or without the immature Łeba-8 sample, as exemplified in Fig. 11 for Cu. The degree of isomerization or branching is considered a indicator of catalytic cracking of hydrocarbons (e.g., Jurg and Eisma, 1964). Butane isomerization as measured by the decimal fraction of *i*- to *n*-butane ($i/[n + i]$) shows no systematic changes or correlations with increasing transition metal content, as exemplified in Fig. 11 for Cu. This isomerization ratio typically decreases with increasing thermal maturity (Su et al., 2006), which explains the highest value for the immature Łeba-8 sample at both experimental conditions.

$\delta^{13}C$ values of generated methane through the butanes have no systematic changes or significant correlations with the transition metals for both experimental conditions as

Table 10
Types, amounts (mg/g TOC), and stable isotopes of gas generated in hydrous pyrolysis experiments at 355 °C/72 h

Samples	Br05	Cu-Wett	Km11	Km16	Ko11	Łeba-8	Mo11	Po08	Po14	R-2a	R-2d	R-3
Components[a]												
Hydrogen	0.41	0.41	0.45	0.32	0.88	0.82	0.49	0.47	0.49	0.28	0.61	0.61
Hyrdogen sulfide	0.25	0.46	1.30	0.13	6.00	24.00	0.00	3.55	2.06	9.01	1.43	1.32
Carbon dioxide	115.94	52.24	145.11	137.59	340.78	632.39	175.66	34.25	184.13	38.25	157.98	198.85
Carbon monoxide	0.01	0.02	0.00	0.00	0.03	0.00	0.00	0.00	0.02	0.00	0.00	0.04
Non-hydrocarbon total	116.61	53.12	146.86	138.05	347.69	657.21	176.16	38.27	186.69	47.54	160.02	200.82
Methane	9.02	7.70	9.92	7.32	11.04	22.99	8.45	15.37	11.43	10.83	13.20	11.95
Ethane	7.44	5.99	7.52	5.34	7.25	14.06	6.95	13.32	9.06	9.17	10.71	9.61
Propane	6.46	5.31	6.45	5.20	7.96	14.67	6.58	9.68	7.87	7.18	9.15	8.53
Propene	0.00	0.00	0.00	0.00	0.09	0.00	0.00	0.00	0.00	0.01	0.00	0.00
n-Butane	3.01	2.55	2.69	2.45	4.03	6.76	3.20	3.62	3.39	2.86	4.03	3.92
i-Butane	0.92	0.76	0.88	0.85	1.41	3.32	0.97	1.31	1.17	1.02	1.37	1.28
n-Pentane	1.18	1.08	0.86	1.01	1.75	2.95	1.34	1.18	1.21	0.78	1.46	1.53
i-Pentane	0.47	0.53	0.47	0.49	0.87	2.21	0.58	0.63	0.63	0.42	0.76	0.74
Hydrocarbon total	28.51	23.91	28.79	22.66	34.41	66.96	28.07	45.11	34.76	32.26	40.68	37.56
Dryness ($C_1/[C_1 - C_4]$)	0.336	0.345	0.361	0.346	0.348	0.372	0.323	0.355	0.347	0.349	0.343	0.339
Ethane/propane	1.151	1.128	1.166	1.027	0.911	0.958	1.055	1.376	1.151	1.278	1.170	1.126
$C_3/[C_1 + C_3]$	0.418	0.408	0.394	0.415	0.419	0.390	0.438	0.386	0.408	0.399	0.409	0.417
$C_4/[C_1 + C_4]$	0.304	0.300	0.265	0.311	0.330	0.305	0.331	0.243	0.285	0.264	0.290	0.303
$i/(n + i)$ Butanes	0.234	0.230	0.248	0.256	0.259	0.329	0.233	0.266	0.256	0.263	0.254	0.246
Methane $\delta^{13}C$[b]	−42.0	−40.2	−41.5	−40.7	−41.8	−38.1	−42.4	−41.4	−39.6	−41.8	−41.0	−41.4
Methane δD[c]	−267.0	−304.0	−307.0	−322.0	−303.0	−338.0	−319.0	−340.0	−290.0	−325.0	−317.0	−320.0
Ethane $\delta^{13}C$[a]	−32.9	−32.2	−32.2	−32.4	−33.2	−32.0	−33.4	−32.2	−32.7	−32.8	−32.7	−32.5
Propane $\delta^{13}C$[a]	−31.3	−30.1	−31.0	−31.2	−32.2	−31.6	−31.5	−31.1	−31.9	−32.0	−31.7	−31.7
n-Butane $\delta^{13}C$[a]	−29.4	−28.5	−29.2	−28.9	−30.6	−30.6	−30.1	−29.8	−29.6	−29.7	n.a.	−30.1
i-Butane $\delta^{13}C$[a]	−28.5	−26.9	−28.3	−28.3	−29.4	−29.5	−29.8	−27.6	−29.0	−28.1	n.a.	−29.3
$CO_2\delta^{13}C$[a]	0.6	−7.4	2.7	2.3	1.6	−1.3	2.6	−10.4	2.2	−6.8	n.a.	2.1

n.a., not analysed.
[a] Ethene, butenes, neopentane, cycopentane, hexanes, and heptanes less than 0.005 mg/g TOC.
[b] ‰ versus V-PDB.
[c] ‰ versus SMOW.

exemplified in Fig. 12 for Cu. These values and the ^{12}C depletion with increasing carbon number of the gases are indicative of thermogenic gases (Whiticar, 1994). The variations in the differences between the $\delta^{13}C$ values of the different gas components are typical of natural gases (Whiticar, 1994), and they have no systematic changes or significant correlations with the transition metals. Compared with the gases generated in the 330 °C experiments, methane generated in the 355 °C experiments is consistently depleted in ^{13}C and the other hydrocarbon gases are nearly the same or enriched in ^{13}C (Fig. 13). δD values of the methane (Tables 9 and 10) also show no systematic changes or significant correlations with the transition metals (Table 6). The high D depletion for all the generated methane has been attributed in a previous study to the contribution of hydrogen from D-depleted distilled water used in the experiments (Kotarba and Lewan, 2004). With the exception of the Łeba-8 sample, methane generated in the 355 °C experiments is more depleted in D than methane generated in the 330 °C experiments. This depletion indicates that water-derived hydrogen may become a more important source of methane hydrogen with increasing thermal maturation.

Sufficient experiments to obtain gas generation rates were not conducted in this study. However, pseudo-rate constants for methane and ethane generation at 330 °C were calculated by assuming maximum yields at 355 °C for 72 h and first-order reaction rates. These pseudo-rate constants are not applicable to gas generation under geological heating rates, but they do allow relative comparisons for rocks with varying transition metal concentrations. The calculated rates for 330 °C showed no increase with increasing transition metals, as exemplified by Cu in Fig. 14.

The yields of immiscible oil expelled during the experiments are given in Table 11. These yields show no systematic changes or significant correlations with the transition metals as exemplified by Cu in Fig. 15. As expected from previous studies (Lewan, 1985, 1997), the expelled immiscible oil yields from the 355 °C experiments are higher than those generated in the 330 °C experiments with the former typically being greater by a factor of two (Fig. 16). Excluding the immature Łeba-8 sample, deviations from this value show no correlation with the transition metal contents. Assuming an API gravity of 25 for all of the oils, gas/oil ratios (GORs) were calculated and are given in Table 11. The GORs for the 355 °C experiments are typically the same or greater than those for the 330 °C experiments with the exception of sample R-2d (Fig. 15). The GORs at both experimental temperatures are similar to those reported for hydrous pyrolysis of Type-II kerogen in the New Albany Shale at experimental temperatures between 330 and 365 °C for 72 h (Lewan and Henry, 1999). Similar to the yields of expelled immiscible oil, there are no systematic

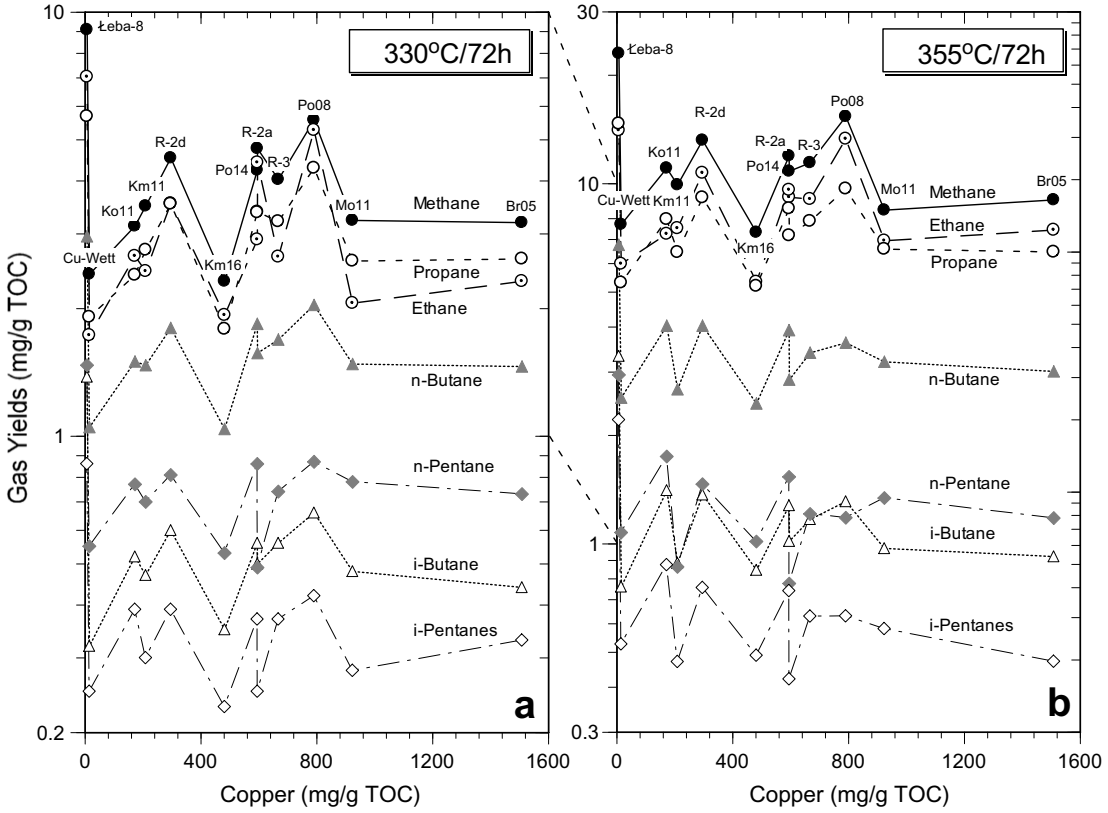

Fig. 8. Bivariate plot of Cu content of the samples on a TOC basis versus hydrocarbon gas yields from experiments at **(a)** 330 °C and **(b)** 355 °C after 72 h. Sample designations are given above symbols for methane and translate vertically for the other gas components.

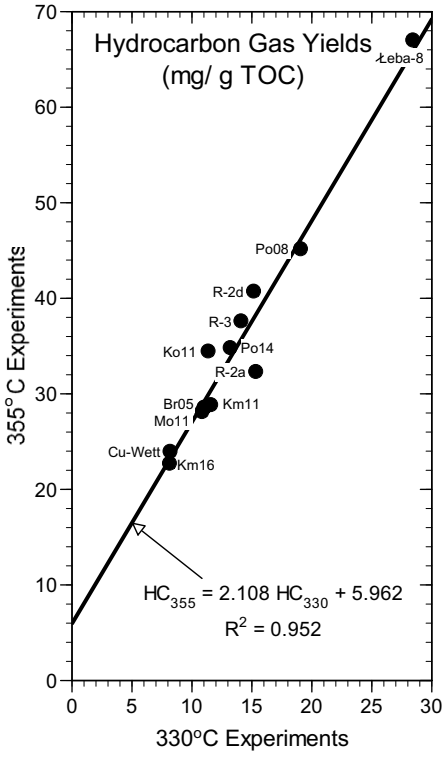

Fig. 9. Bivariate plot of total hydrocarbon gas yields from 330 °C experiments versus those from 355 °C experiments.

changes or significant correlations between GOR and the transition metals as exemplified for Cu in Fig. 15.

4. DISCUSSION

The high and variable transition-metal contents of the Kupferschiefer samples used in this study provide an opportunity to evaluate their catalytic role in gas generation. Although these rocks are enriched in transition metals due to epigenetic hydrothermal fluids (Wodzicki and Piestrzyński, 1994; Piestrzyński et al., 2002), they are otherwise representative of other black shales in their SiO_2/Al_2O_3 ratios (Fig. 2), varying carbonate contents (Figs. 2 and 3b), and S_{total}/TOC ratios (Fig. 4c). The transition metals are dispersed with organic matter of the same kerogen type (i.e., Type-II kerogen) within rocks of similar thermal maturities. Contacts between organic matter and metals are enhanced by the rock matrix becoming impregnated with polar-rich bitumen during the early stages of kerogen decomposition. In addition, this bitumen impregnation reduces liquid water films or pore fillings that could act as barriers between potential organic matter contacts with metals. Another favorable attribute of these samples is their exceptionally high concentrations of Cu, which is a versatile transition metal for various industrial catalytic gas reactions involving methanol formation (Olah and Molnár, 2003, p. 114), oxidation of ethene (Somorjai, 1994, p. 460), ethene hydrogenation (Masel, 2001, p. 879), and eth-

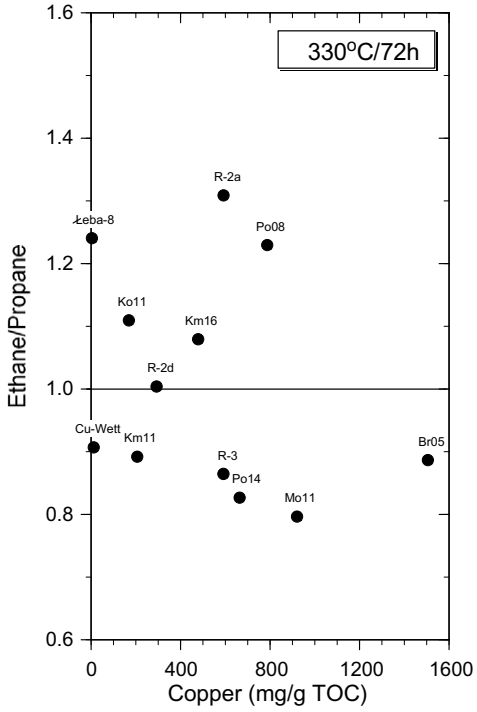

Fig. 10. Bivariate plot of ethane/propane ratio of gases generated at 330 °C after 72 h versus Cu content of the samples on a TOC basis. Sample designations are given above symbols.

ane hydrogenolysis (Bond, 2005, p. 537). The Arrhenius plot in Fig. 17 shows the significance of metal catalysis in methane generation by ethane hydrogenolysis over Ni^o compared to methane generation from non-catalytic thermal decomposition of Type-II kerogen (Knauss et al., 1997). Catalytic rates of methane generation remain orders of magnitude greater than non-catalytic methane generation at subsurface temperatures (<200 °C), as well as at the experimental temperatures used in this study. With these favorable attributes for catalysis, the lack of any observed catalytic effects on gas generation in this study indicates the metals are not in the proper form to be effective catalysts or their exposures are readily poisoned by polar-rich bitumen impregnating the rock matrix.

With the exception of activated NiO, catalytic transition metals are typically in their zero-valence state (i.e., Cu^o, Ni^o, Fe^o, Co^o). Eh–pH diagrams in Fig. 18 show that within the stability limits of water at 25 °C, sea water concentrations of metals and sulfur (Krauskopf, 1967, Appendix II), and a total pressure of 1 atm, only copper occurs in its zero-valence state (i.e., Cu^o; hatched field in Fig. 18a). The Eh–pH limits between the water stability limits can be better defined by the pH and Eh measurements of marine and marginal marine sediments (Baas Becking et al., 1960), which are outlined by a dashed line labeled "**ms**" in Fig. 18. This outlined field is further constrained by negative Eh values that reflect the reducing conditions in which source rocks induce or are deposited (e.g., Lewan, 1984). Within these

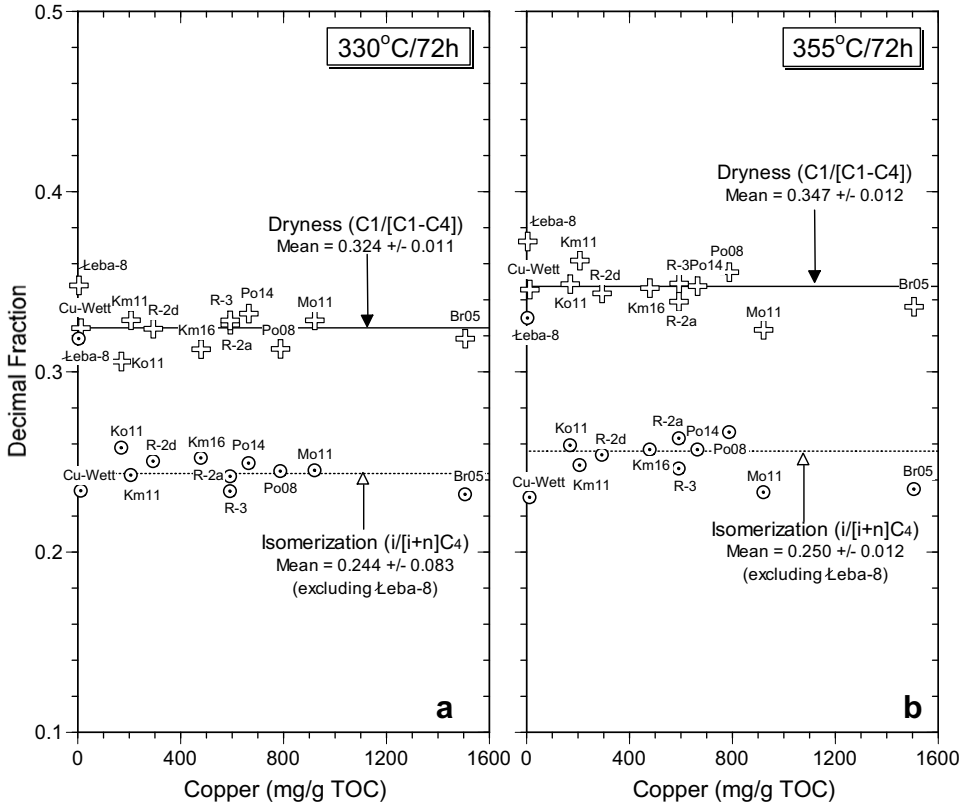

Fig. 11. Bivariate plot of Cu content of the samples on a TOC basis versus methane dryness (open plus signs) and butane isomerization (open circles with central dot) of gases generated at **(a)** 330 °C and **(b)** 355 °C after 72 h. Sample designations are given adjacent to symbols.

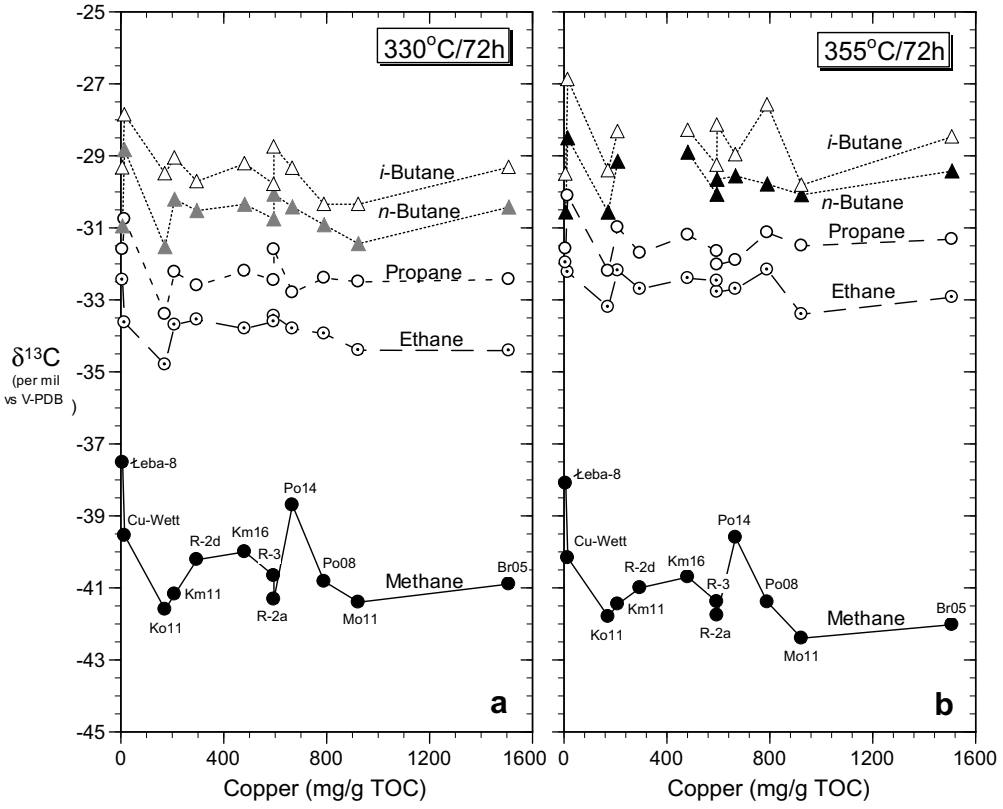

Fig. 12. Bivariate plot of Cu versus $\delta^{13}C$ of methane, ethane, propane, *n*-butane, and *i*-butane generated at **(a)** 330 °C and **(b)** 355 °C after 72 h. Sample designations are given adjacent to symbols for methane and translate vertically for the other gas components.

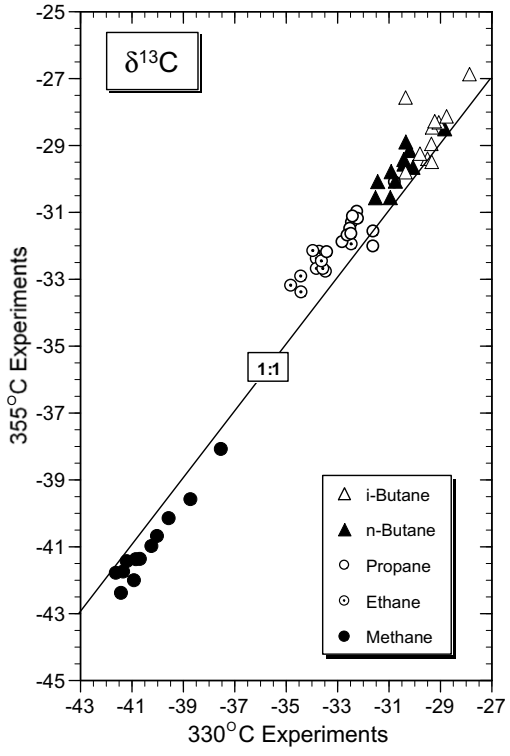

Fig. 13. Bivariate plot of the $\delta^{13}C$ of methane, ethane, propane, and butanes generated at 330 °C versus those generated at 355 °C for 72 h.

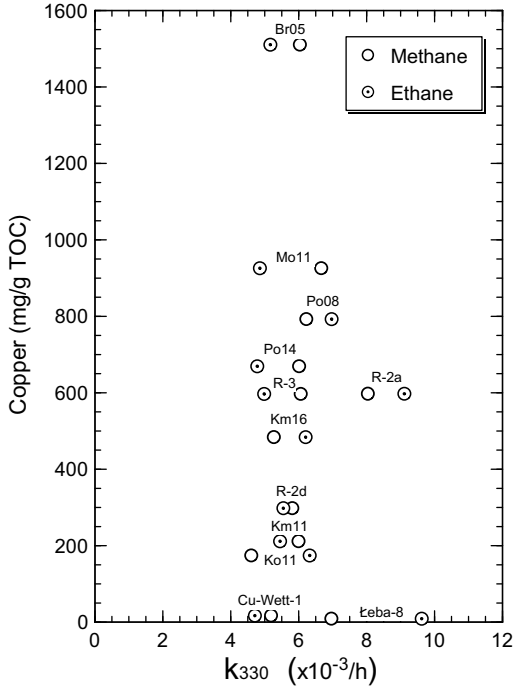

Fig. 14. Bivariate plot of pseudo-rate constants for methane and ethane generation at 330 °C versus Cu content.

Table 11
Expelled immiscible oil yields and gas/oil ratios for experiments at 330 °C and 355 °C for 72 h

Conditions	330 °C/72 h		355 °C/72 h	
	Immiscible oil (mg/g TOC)	Gas:oil ratio[a] (scf/bbl)	Immiscible oil (mg/g TOC)	Gas:oil ratio[a] (scf/bbl)
Sample				
Br05	43.5	1017	114.4	1076
Cu-Wet	15.6	2119	38.9	2648
Km11	47.2	1006	113.8	1137
Km16	38.2	861	87.2	1115
Ko11	51.6	869	154.2	938
Łeba-8	130.2	927	221.7	1305
Mo11	54.0	806	118.8	991
Po08	63.8	1255	171.2	1198
Po14	59.7	907	171.2	892
R-2a	80.3	833	173.5	838
R-2d	56.6	1109	183.2	971
R-3	64.3	898	146.0	1114

[a] Calculated for methane through butanes and assuming an oil API gravity of 25.

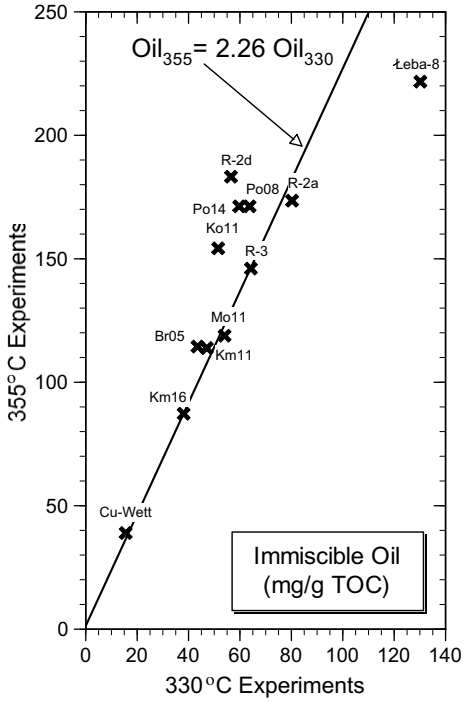

Fig. 16. Bivariate plot of expelled immiscible oil yields of the 330 °C experiments versus those of the 355 °C experiments.

natural Eh–pH limits, Cu^o is present, but Ni^o, Co^o, and Fe^o are not (Fig. 18). Magnitude differences in concentrations (Garrels and Christ, 1965), temperatures between 0 and 50 °C (Garrels and Christ, 1965), and pressures within tens of atmospheres have only a minor affect on the calculated stability fields (Evans and Garrels, 1958; Brookins, 1988). As a result, no organic-rich sediment or its subsequent thermally immature source rock is likely to have zero-valence metals with the exception of Cu.

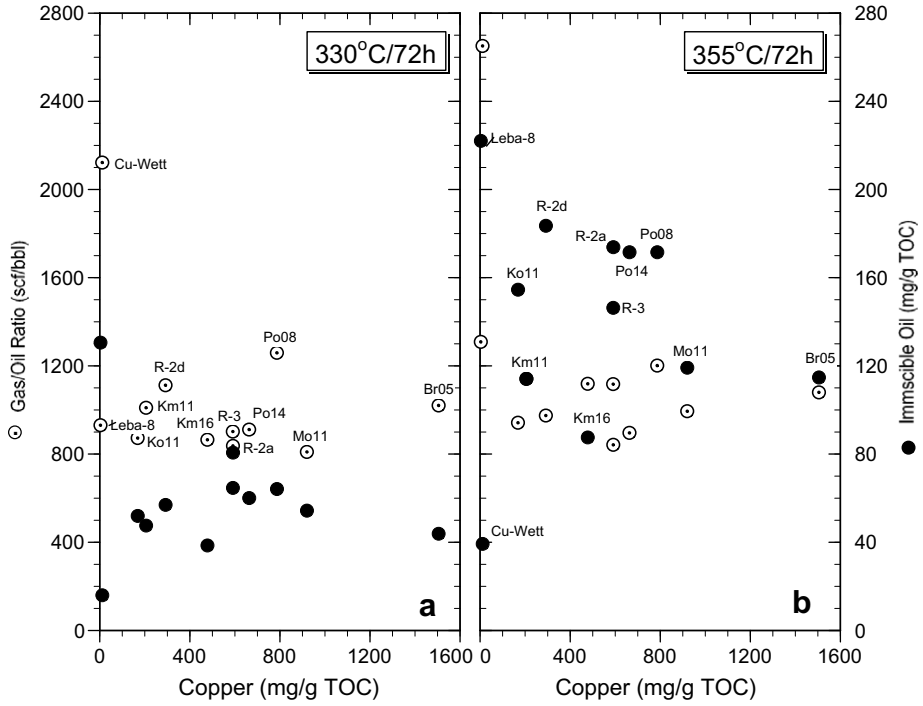

Fig. 15. Bivariate plot of Cu versus yield of expelled immiscible oil and gas/oil ratios (GOR) for experiments at **(a)** 330 °C and **(b)** 355 °C after 72 h. Sample designations are given adjacent to symbols for GOR and translate vertically for the expelled immiscible oil yields.

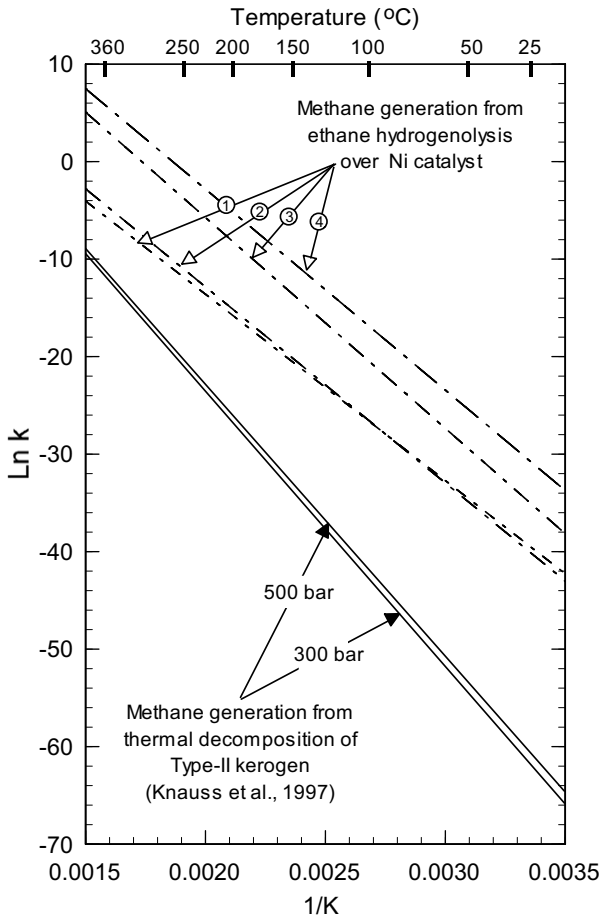

Fig. 17. Arrhenius plot comparing the rate relationships of methane generated by ethane hydrogenolysis over Ni^o catalysts and methane generated by the thermal decomposition of Type-II kerogen (Knauss et al., 1997). Catalysis lines include unsupported Ni^o powder as reported by (1) Freel and Galwey (1968), (2) Sinfelt et al. (1972), and (3) Babernics et al. (1976), and SiO_2 supported 5% Ni^o reported by (4) Sinfelt (1973). Reported frequency factors for the catalytic relationships were converted from molecules/cm^2/s to first-order units in s^{-1} by a factor of 10^{15} metal surface atoms/cm^2 as prescribed by Sinfelt (1991) to facilitate comparisons with non-catalytic gas generation. Relationships for methane generated from thermal decomposition of Type-II kerogen in New Albany Shale by hydrous pyrolysis at 300 and 500 bar using mean activation energies of Gaussian distributions (56.1 and 55.4 kcal/mol, respectively), fixed frequency factor (2×10^{14} s^{-1}), and first-order reactions (Knauss et al., 1997, Table 5).

In addition to zero-valence metals like Ni, Fe, and Co not occurring during the deposition or initial lithification of organic-rich sediments, they are also not thermodynamically stable at higher temperatures representing petroleum generation in sedimentary basins. Eh-ph diagrams similar to those in Fig. 18 for Ni, Fe, and Co have also been constructed for temperatures up to 300 °C, three-orders of magnitude higher metal molar concentrations than sea water, and H_2 partial pressures as high as 100 bars (not shown). None of the Fe diagrams ($\Sigma Fe = 10^{-6.75}$ to $10^{-3.75}$ M) show the intersection of the lower stability limit of water at H_2 partial pressures of 100 bars or less with the boundary for zero-valance metals at pH values less than 14 at 100, 200, or 300 °C. The Co and Ni diagrams ($\Sigma Co = 10^{-8.77}$ to $10^{-5.77}$ M, $\Sigma Ni = 10^{-7.47}$ to $10^{-4.47}$ M) show the intersection of the lower stability limit of water at H_2 partial pressures of 100 bar or less with the boundary for zero-valance metals at or above pH values of 11.2 and 12.0, respectively, at 100 °C, 9.5 and 10.0, respectively, at 200 °C, and 8.3 and 8.8, respectively, at 300 °C. Calculated *in situ* pH values reported for subsurface formation waters at temperatures as high as 162 °C are typically between 5 and 7 (Palandri and Reed, 2001), which suggests that the high pH values under which Co^o and Ni^o are stable are not likely during petroleum formation in the subsurface.

Fig. 19 shows the Eh difference between zero-valance metal boundaries with their sulfides and the lower stability limit of water at a pH of 6 for temperatures between 25 and 300 °C at H_2 partial pressures of 1, 10, and 100 bars. All of the curves indicate that the lower stability limit for water is never reducing enough to coincide or intersect with the stability field for zero-valence metals ($\Delta Eh \leqslant 0$) of Ni, Fe, and Co. Drummond (1981, p. 64) states that H_2 is most prevalent in reduced high-temperature hydrothermal and magmatic systems, but is unlikely to exceed 100 atm (i.e., 101.3 bars) under natural conditions. Extrapolation of these curves in Fig. 19 to the experimental temperatures used in this study also indicate that zero-valence metals of Ni, Fe, or Co are not thermodynamically stable. The highest H_2 partial pressures for the hydrous pyrolysis experiments calculated from Henry's law constants compiled by Drummond (1981) were only 0.13 and 0.12 bars after 72 h at 330 and 355 °C, respectively. As shown by the extrapolations in Fig. 19, these H_2 partial pressures are not sufficient for Ni, Fe, and Co to occur in their zero-valence state during the experiments. These relationships are not affected by three order-of-magnitude increases in metal concentrations at pH values greater than 3, and sulfur concentrations greater than that of seawater only lower the upper Eh–pH boundary of the field for zero-valence metal.

Copper sulfides (e.g., chalcocite, Cu_2S; and covellite, CuS) are the most common copper minerals identified in the Kupferschiefer, but occurrences of zero-valence native copper (Cu^o) have also been reported (Haranczyk, 1972; Sawłowicz, 1990a). These occurrences of zero-valence copper and other transition metals (Ag^o, Pb^o, Au^o) indicate that microcosms with low sulfide activity or strong reducing conditions may occur within the Kupferschiefer (Sawłowicz, 1990b). Petrographic studies under reflected light and X-ray diffraction analysis of the samples detected no native copper in the samples, with detection limits of ~2 μm and ~0.5 wt%, respectively. If some native copper below these detection limits existed in the samples, their catalytic effect would be restricted to these isolated microcosms. In addition, Cu^o like other zero-valence transition metals (e.g., Ni^o, Somorjai, 1994, p. 592) is a structure sensitive catalyst, which means that catalytic rates decrease significantly with decreasing particle size (Masel, 2001, p. 870). The catalytic effectiveness of these microcosms of zero-valence transition metals may also be reduced by bitumen poisoning. During the early stages of thermal maturation, oil-prone kerogen

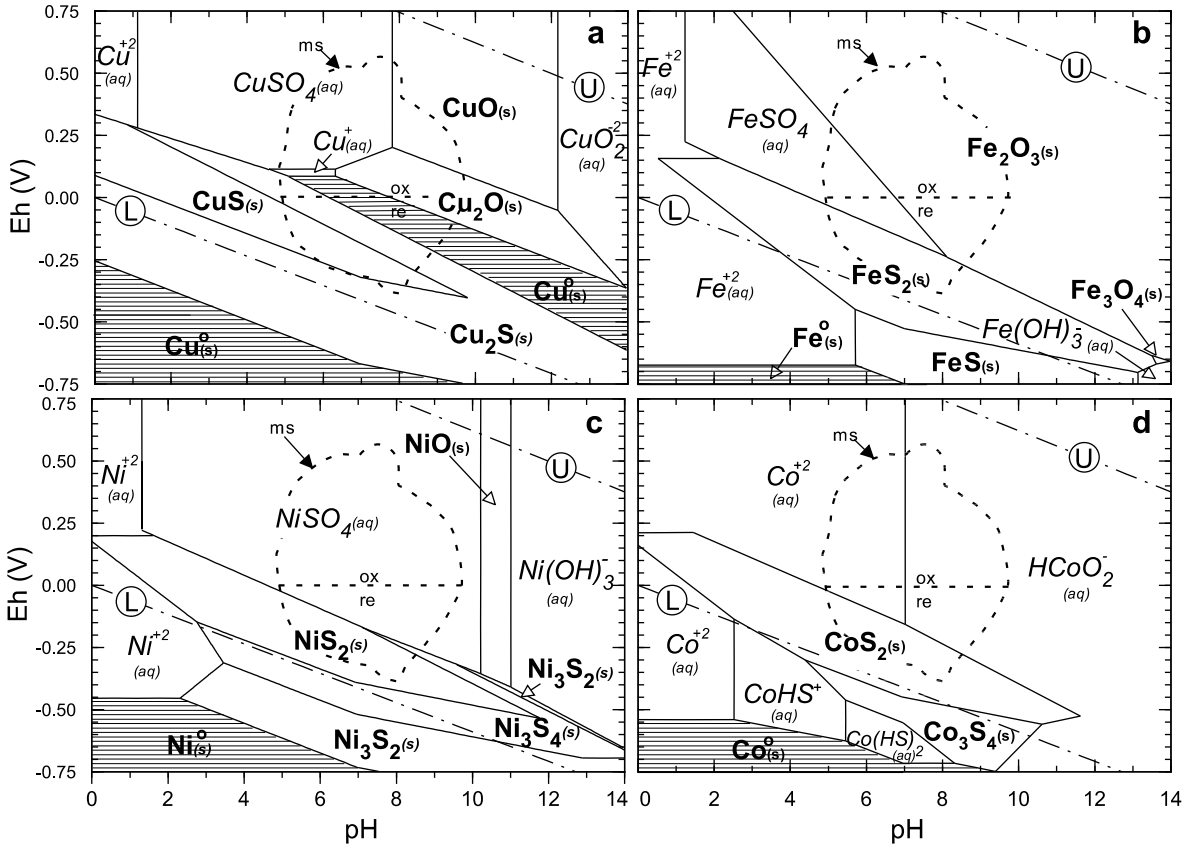

Fig. 18. Eh–pH diagrams for (a) copper, (b) iron, (c) nickel, and (d) Co at 25 °C, 1 atm total pressure, and seawater concentrations (Cu = 0.003; Co = 0.0001; Fe = 0.01; Ni = 0.002; total S = 885 in ppm from Krauskopf, 1967, Appendix III). Stability fields were calculated with Geochemist's Workbench 6.0 with the "thermo.com.v8.r6+.dat" thermodynamic data set. Broken lines labeled U and L represent stability limits for water at 25 °C and 1 atm of pressure (Garrels and Christ, 1965). Dashed outline represents field for marine and marginal marine sediments as reported by Baas Becking et al. (1960). Horizontal dashed line at an Eh of zero denotes the boundary between reducing (re) and oxidizing (ox) redox conditions.

initially decomposes to polar-rich bitumen that impregnates the micoporosity and partings of a source rock (Lewan, 1987, 1993). This impregnation is a result of the kerogen-to-bitumen reaction having an overall net volume increase that is observed in petrographic studies (Lewan, 1987, 1993) and accounts for the development of high well-log resistivities reported in maturing subsurface source rocks (Meissner, 1978; Schmoker and Hester, 1990; Passey et al., 1990; Morel, 1999). This bitumen impregnation of the matrix is likely to maximize contacts between the organic matter and potential native-copper microcosms, but the polar composition of the bitumen would readily poison these microcosms and limit their effectiveness as catalysts.

In addition to zero-valence metals, activated NiO has been shown to be an effective catalyst in generating a methane-rich gas from *n*-dodecene-1 in the presence of H_2 gas at 200 °C for 24 h (Mango, 1996). The NiO is activated by flowing H_2 (at 1 atm, 1 mL/min) over it at 350 °C for 24 h. Activated NiO on a silica gel has also been shown to be an effective catalyst (Mango, 1996). Relating these experimental results to natural gas generation is difficult because the NiO mineral, Bunsenite, is reported in high temperature regimes involving hydrothermal or metamorphic conditions (Anthony et al., 1997) and in converter slags from smelting of copper ores (Wearing, 1984). As shown in Fig. 18c, it is only thermodynamically stable at high pH conditions (>10 and <11), which are not commonly present in marine or marginal marine sediments. Similar to zero-valence metals, the effectiveness of traces of NiO as a catalyst in petroleum source rocks will be limited to microcosms and poisoned by bitumen impregnation.

Transition metals may also be sequestered in clay minerals of shales and petroleum source rocks. As shown in Table 12, there are significant positive correlations between Al_2O_3 and Cr, Ni, Ag, Cu, and V. These metals can be accommodated within the octahedral layer of the clay minerals (Decarreau, 1985). Clay mineral studies report that most of the nickel resides as a nickelous cation (Ni^{2+}) in the octahedral layer (Edel'shteyn and Zuzuk, 1974; Vieira Coelho et al., 2000a,b). Its substitution for aluminum within this layer may result in a charge imbalance that is translated to the surface of the clay mineral, which provides catalytic activity to the clay mineral for hydroisomerization of normal alkanes to branched alkanes (Swift and Black, 1974; Heinermann et al., 1983; Robschlager et al., 1984). In this respect, the clay mineral surface is the catalyst and

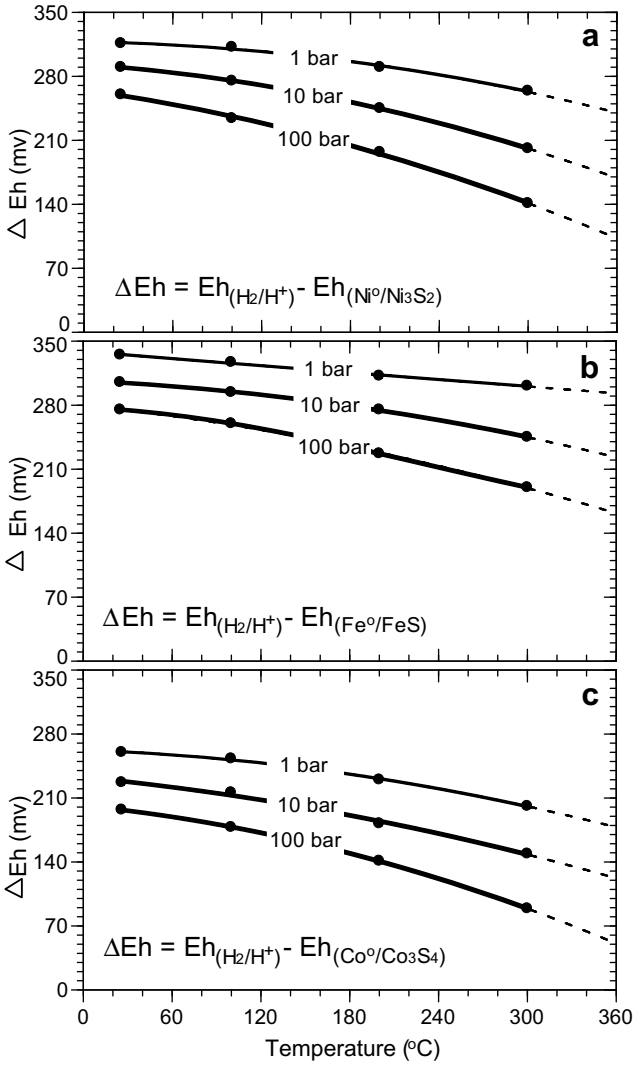

Fig. 19. Plots showing the mV difference in Eh at a pH of 6 between the lower stability boundary of water ($H_{2(g)} = 2H^+ + 2e^-$) and the boundary between zero-valence metals (Ni^o, Fe^o, and Co^o) and their stable sulfides (Ni_3S_2, FeS, and Co_3S_4, respectively) at temperatures from 25 to 300 °C and H_2 partial pressures of 1, 10, and 100 bar. Thermodynamic data, concentrations, and calculations are the same as those used in the construction of Fig. 17, but at higher temperatures and pressures. H_2 partial-pressure curves are polynomial expressions based on calculated values at 25, 100, 200, and 300 °C. The polynomial expressions were used to extrapolate the Eh differences to 360 °C. (a) Eh differences between the Ni^o/Ni_3S_2 (i.e., heazlewoodite) boundary and lower stability boundary of water. (b) Eh differences between the Fe^o/FeS (i.e., troilite) boundary and lower stability boundary of water. (c) Eh differences between the Co^o/Co_3S_4 (i.e., linnaeite) boundary and lower stability boundary of water. The lowest temperature calculated for this plot was 26 °C to avoid the occurrence of an intermediate aqueous field of $Co(HS)_2$ that occurs at temperatures less than 26 °C. Eh–pH diagrams (not shown) upon which these relationships are based, were constructed using Geochemist's Workbench® Release 6.0 program with the thermodynamic dataset "thermo.com.V8.R6+.data base".

not the cationic metal within the mineral lattice. Vanadium as a cation (V^{+3}) has also been shown to reside in the octahedral layer of clay minerals (Meunier, 1994), which also renders it ineffective as a metal catalyst. Chromium oxide/hydroxide and native copper inclusions have been observed in some clay minerals (Fabbri et al., 1989 and Ahn et al., 1997; respectively). However, the submicron size and limited occurrence of these inclusions within clay-mineral lattices makes their exposure and effectiveness as a catalyst unlikely in bitumen impregnated petroleum source rocks. The significant positive correlation between Ag and Al_2O_3 is difficult to explain by substitution in the octahedral layer of clay minerals. Within the Eh–pH stability field for water, Ag occurs as a monovalent cation that under the most ideal setting does not appear to substitute into clay minerals (e.g., Delain et al., 1992).

Some transition metals may be concentrated in petroleum source rocks as metallo-organic complexes during early diagenesis (Lewan and Maynard, 1982). Within naturally occurring organic matter, nickel or vanadium and to a lesser extent iron and copper are consistently the most abundant transition metals in these complexes (e.g., Hodgson, 1954; Filby and Van Berkel, 1987). Their high thermal stability and acid resistant character suggests they occur

Table 12
Linear regression correlations (R) and expresions between transition metals and Al_2O_3

Metal	*R*	Slope	Intercept
Cr	0.902	28.00	−58.1
Ni	0.878	58.41	−219.5
Ag	0.860	36.62	−211.0
Cu	0.846	1.87	−13.7
V	0.813	170.19	−395.2
Mo	0.504	NS[a]	NS[a]
Zn	0.459	NS[a]	NS[a]
Cd	0.432	NS[a]	NS[a]
Hg	0.408	NS[a]	NS[a]
Pb	0.319	NS[a]	NS[a]
Co	0.277	NS[a]	NS[a]

[a] NS, not significant at confidence intervals of 99% for 12 samples based on the *F* test (Crow et al., 1960).

within tetrapyrrole (porphyrin and non-porphyrin) complexes (Lewan and Maynard, 1982). Both nickel and vanadium occur in the tetrapyrrole complexes as nickelous (Ni^{2+}) and vanadyl (VO^{2+}) cations (Erdman et al., 1956; Fleischer, 1963). Porphyrins with these two metals and ferric iron (Fe^{+3}) have been reported in the Kupferschiefer of Germany (Eckardt et al., 1989; Wolf et al., 1989), but only vanadyl and ferric iron porphyrins have been reported in the mineralized Kupferschiefer of Poland (Kucha et al., 1983; Czechowski, 2000). Experimental data reported by Mango (1996) show that nickelous- and vanadyl-porphyrins have no significant catalytic activity in methane generation from alkenes. This ineffectiveness as a catalyst may be the result of the metals occurring as cations strongly bound to the central regions of large tetrapyrrole molecules.

5. CONCLUSIONS

The high and varying metal content of the Permian Kupferschiefer samples used in this study provided an opportunity to evaluate the catalytic effect of transition metals on gas generation from petroleum source rocks. Although their high metal contents were introduced by epigenetic hydrothermal fluids, the samples were only marginally matured and the metal phases are similar to those commonly associated with syndepositional metal enrichment in petroleum source rocks. Hydrous pyrolysis of the samples at 330 and 355 °C for 72 h generated gases with no enhanced yields, methane enrichment (dryness), or generation rates that could be attributed to concentrations or types of transition metals present. This lack of catalytic activity is attributed to the transition metals not occurring in the appropriate form to serve as effective catalysts or their exposures are readily poisoned by polar-rich bitumen impregnating the rock matrix during early thermal maturation. Most of the transition metals with the greatest catalytic potential (i.e., Cu, Fe, Co, and Ni) are chalcophyllic and occur in high concentrations as a result of metal sulfide formation during deposition of marine and marginal-marine source rocks. Only copper has the potential to occur as a zero-valence metal (Cu^o) under some depositional settings. In spite of the possibility that some Cu^o may exist in these copper-rich rocks, generated gases showed no signs of catalytic activity in the hydrous pyrolysis experiments. This lack of catalytic activity by potential zero-valence metals may be attributed to the poisoning of catalytic sites by polar-rich bitumen that impregnates the matrix of source rocks during the early stages of petroleum generation. In addition to occurring as sulfides, some of the transition metals (Cr, Ni, Cu, and V) may reside in the octahedral layer of clay minerals. Their substitution in this layer for aluminum may result in a charge imbalance on the clay-mineral surface, but the direct catalytic effectiveness of the metal cation within the lattice is unlikely. Similarly, metal cations strongly bound to the central regions of large tetrapyrrole complexes within the organic matter are not effective catalysts as demonstrated in previous experiments (Mango, 1996). These results indicate that transition metals are not catalytic in petroleum source rocks, and additional research remains to be conducted to understand the controls on yields, composition, and timing of natural gas generation.

ACKNOWLEDGMENTS

This research was undertaken as part of the Polish Ministry of Science and Higher Education Grant 3473/C-T12-6/2004 and the Polish Copper Company KGHM Polska Miedz S.A. The efforts of Dr. Peer Hoth (Bundesanstalt fur Geowissenschaften und Rohstoffe, Berlin) in providing a Kupferschiefer sample rich in zinc (Cu-Wett) is acknowledged and appreciated. Analytic work by A. Warden of the USGS on gas compositions and by T. Kowalski and H. Zych at AGH-University of Science and Technology on stable isotope determinations is gratefully acknowledged. The authors are also grateful for the X-ray diffraction analysis by J. Azain and W. Betterton of the USGS and their efforts to detect native copper. M. J. Pawlewicz of the USGS is acknowledged for his assistance in obtaining polished sections of the samples and standards for microscopic analyses of the ore minerals. Vitrinite reflectance measurements by Prof. Wagner of AGH-University of Science and Technology are gratefully appreciated.

Diligence in providing high quality graphics to this study by W. Więcław is acknowledged and appreciated. The authors appreciate the helpful comments and suggestions to earlier versions of the manuscript by John B. Curtis of the Colorado School of Mines, and Geoffrey Ellis and Richard Keefer of the USGS. The manuscript also benefited from discussions on rates of catalytic reactions with John Sinfelt of ExxonMobil (retired), Geoffrey Bond of Brunel University (emeritus), and Tracy Gardner of the Colorado School of Mines. Lastly, the authors are appreciative of the two anonymous reviewers, Frank Mango, and Jeffrey Seewald for their comprehensive formal reviews.

REFERENCES

Ahn J. H., Xu H. and Buseck P. R. (1997) Transmission electron microscopy of native copper inclusions in illite. *Clays Clay Miner.* **45**, 295–297.

Amrani A., Lewan M. D. and Aizenshtat Z. (2005) Stable sulfur isotope partitioning during simulated petroleum formation as determined by hydrous pyrolysis of Ghareb Limestone, Israel. *Geochim. Cosmochim. Acta* **69**, 5317–5331.

Anthony J. W., Bideaux R. A., Bladh K. W. and Nichols M. C. (1997) *Handbook of Mineralogy*, 28 pp.

Baas Becking L. G. M., Kaplan I. R. and Moore D. (1960) Limits of natural environments in terms of pH and oxidation–reduction potential. *J. Geol.* **68**, 243–284.

Babernics L., Guczi L., Matusek K., Sárkány A. and Tétény, P. (1976) Comparative study of metal–hydrocarbon interaction and hydrogenolysis. In *Proceedings of the Sixth International Congress on Catalysis* (London), vol. 1, pp. 456–468.

Baskin D. K. (1997) Atomic H/C ratio of kerogen as an estimate of thermal maturation and organic conversion. *Am. Assoc. Petrol. Geol. Bull.* **81**, 1437–1450.

Bastin E. S. (1933) The chalcocite and native copper types of ore deposits. *Econ. Geol.* **28**, 407–446.

Bechtel A., Sun Y., Püttmann W., Hoernes S. and Hoefs J. (2001) Isotopic evidence for multi-stage base metal enrichment in Kupferschiefer from the Sangerhausen basin, Germany. *Chem. Geol.* **176**, 31–49.

Berner R. A. (1984) Sedimentary pyrite formation: an update. *Geochim. Cosmochim. Acta* **48**, 605–615.

Bond G. C. (2005) *Metal-catalysed Reactions of Hydrocarbons*. Springer, New York, 666 pp.

Brookins D. G. (1988) *Eh–pH Diagrams for Geochemistry*. Springer-Verlag, Berlin, 176 pp.

Cai J., Bao Y., Lu L., Xu J. and Zheng D. (2008) *Occurrence and its Implications of Organic Matter Bound in Interlayer of Montmorillonite in Source Rocks*. American Association of Petroleum Geologists Annual Convention, April 20–23, San Antonio, TX, Abstracts v. 17.

Chen P.-Y. and Shaffer N. R. (1979) Petrography and Mineralogy of Mudstones of the Carbondale Group (Middle Pennsylvanian), Indiana: Neuvième Congrès International de Stratigraphie et de Gèologie du Carbonifère, Washington and Champaign-Urbana, May 17–26, 1979, Compte Rendu, vol. 3, pp. 641–655.

Clarke F. W. (1924) The data of geochemistry, 5th Edition, Chapter XIII. Sedimentary and detrital rocks. *U.S. Geol. Surv. Bull.* **770**, 543–593.

Crow E. L., Davis F. A. and Maxfield M. W. (1960) *Statistics Manual*. Dover Publications, New York, 288 pp.

Cubitt J. (1979) The geochemistry, mineralogy and petrology of Upper Paleozoic shales of Kansas. *Kansas State Geol. Surv. Bull.* **217**, 117.

Cullers R. L. (1994) The controls on the major and trace element variation of shales, siltstones, and sandstones of Pennsylvanian–Permian age from uplifted continental blocks in Colorado to platform sediments in Kansas, USA. *Geochim. Cosmochim. Acta* **58**, 4955–4972.

Czechowski F. (2000) Metalloporphyrin composition and a model for the early diagenetic mineralization of the Permian Kupferschiefer, SW Poland. In *Organic Matter and Mineralization: Thermal Alteration, Hydrocarbon Generation, and Role in Metallogenesis* (eds. M. Glikson and M. Mastalerz). Kluwer Academic, London, pp. 243–259.

Decarreau A. (1985) Partitioning of divalent transition elements between octahedral sheets of trioctahedral smectites and water. *Geochim. Cosmochim. Acta* **49**, 1537–1544.

Delain F., Jie Y. and Tiebing L. (1992) Black shale series-hosted silver–vanadium deposits of the upper Sinian Doushantuo Formation, western Hubei Province, China. *Explor. Min. Geol.* **1**, 29–38.

Downorowicz S. (1996) Occurrence of natural gas and oil (Występowanie gazu ziemnego i ropy naftowej). In *Mongrafia KGHM Polska Miedź S.A., CBPM, Cuprum, Wrocław* (eds. A. Piestrzyński, A. W. Jasiński, J. Kotlarski, W. Maślanka, S. Siewierski, S. Speczik and Z. Śmieszek), pp. 168–172 (in Polish).

Drummond Jr. S. E. (1981) *Boiling and Mixing of Hydrothermal Fluids: Chemical Effects on Mineral Precipitation*. Pennsylvanian State University, Department of Geosciences, Ph.D. Dissertation, 380 pp.

Eckardt C. B., Wolf M. and Maxwell J. R. (1989) Iron porphyrins in the Permian Kupferschiefer of the Lower Rhine Basin, N.W. Germany. *Org. Geochem.* **14**, 659–666.

Edel'shteyn I. I. and Zuzuk F. V. (1974) On the forms of occurrence of nickel in chlorites. *Geochem. Int.* **11**, 305–313.

Erdman J. G., Ramsey V. G., Kalenda N. W. and Hanson W. E. (1956) Synthesis and properties of porphyrin vanadium complexes. *J. Am. Chem. Soc.* **78**, 5844–5847.

Evans, Jr., H. T. and Garrels R. M. (1958) Thermodynamic equilibria of vanadium in aqueous systems as applied to the interpretation of the Colorado Plateau ore deposits. *Geochim. Cosmochim. Acta* **15**, 131–149.

Fabbri B., Morandi N. and Nannetti M. C. (1989) Abundance of chromium and other transition metals in ceramic clays from Westerwald (GFR). *Appl. Clay Sci.* **4**, 475–484.

Filby R. H. and Van Berkel G. J. (1987) Geochemistry of metal complexes in petroleum, source rocks, and coals: an overview. In *Metal Complexes in Fossil Fuels* (eds. R. H. Filby and J. F. Branthaver). American Chemical Society Symposium Series 344, pp. 2–39.

Fleischer E. G. (1963) The structure of nickel etioporphyrin I. *J. Am. Chem. Soc.* **85**, 146–148.

Freel J. and Galwey A. K. (1968) Hydrocarbon cracking reactions on nickel. *J. Catal.* **10**, 277–289.

Garrels R. M. and Christ C. L. (1965) *Minerals, Solutions and Equilibria*. Harper and Rowley, New York, 453 pp.

Gromet L. P., Dymek R. F., Haskin L. A. and Korotev R. L. (1984) The North American shale composite: its compilation, major and trace element characteristics. *Geochim. Cosmochim. Acta* **48**, 2469–2482.

Hammer J., Roesler H. J. and Gleisberg B. (1988) Neutroenaktivierungs analytische, säulenchromatographische und IR-spektroskopische untersuchungen der bitumensubstanz des Kupferschiefers der Sangerhäuser Mulde (DDR). *Chem. Erde* **48**, 61–78.

Haranczyk C. (1972) Ore mineralization in the lower Permian anoxic sediments of the Fore Sudetic Monocline. *Arch. Mineral.* **30**, 13–171.

Heinermann J. J. L., Freriks I. L. C., Gaaf J., Pott G. T. and Coolegen J. G. F. (1983) The catalytic activity of nickel substituted mica-montmorillonite. *J. Catal.* **80**, 145–153.

Hodgson G. W. (1954) Vanadium, nickel, and iron trace metals in crude oils of western Canada. *Am. Assoc. Petrol. Geol. Bull.* **38**, 2537–2554.

Hunt J. M. (1996) *Petroleum Geochemistry and Geology*. W.H. Freeman and Company, New York, 743 pp.

Jowett E. C., Roth T., Rydzewski A. and Oszczepalski S. (1991) "Background" $\delta^{34}S$ values of Kupferschiefer sulphides in Poland: pyrite–marcasite nodules. *Miner. Deposita* **26**, 89–98.

Jung W. and Knitzschke G. (1976) Kupferschiefer in the German Democratic Republic (GDR) with special reference to the Kupferschiefer deposit in the southeastern Harz foreland. In *Handbook of Strata-Bound and Stratiform Ore Deposits, II. Regional Studies and Specific Deposits. Vol. 6, Cu, Zn, Pb, and Ag deposits* (ed. K. H. Wolf), pp. 353–406.

Jurg J. W. and Eisma E. (1964) Petroleum hydrocarbons: generation from fatty acids. *Science* **144**, 1451–1452.

Keith M. L. and Degens E. T. (1959) Geochemical indicators of marine and fresh-water Sediments. In *Researches in Geochemistry* (ed. P. H. Abelson). John Wiley and Sons, London, pp. 38–61.

Kennedy M. J., Pevear D. R. and Hill R. J. (2002) Mineral surface control of organic carbon in black shale. *Science* **295**, 657–660.

Knauss K. G., Copenhaver S. A., Braun R. L. and Burnham A. K. (1997) Hydrous pyrolysis of New Albany and Phosphoria shales: production kinetics of carboxylic acids and light hydrocarbons and interactions between the inorganic and organic chemical systems. *Org. Geochem.* **27**, 477–496.

Kotarba M. J. and Lewan M. D. (2004) Characterizing thermogenic coalbed gas from Polish coals of different ranks by hydrous pyrolysis. *Org. Geochem.* **35**, 615–646.

Krauskopf K. B. (1967) *Introduction to Geochemistry*. McGraw-Hill Book Company, New York, 721 pp.

Kucha H. (1993) Noble metals associated with organic matter, Kupferschiefer, Poland. In *Bitumens in Ore Deposits* (eds. J. Parnell, H. Kucha and P. Landis). Springer-Verlag, Berlin, pp. 153–177.

Kucha H. and Mayer W. (1996) Geochemistry. In *Monografia KGHM Polska Miedź S.A., Lubin* (ed. A. Piestrzyński), pp. 237–251.

Kucha H., Mayer W. and Piestrzyński A. (1983) Vanadium in the copper ore deposit on the Fore-Sudetic Monocline (Poland). *Mineral. Polon.* **14**, 35–44.

Leventhal J. S. (1983) An interpretation of carbon and sulfur relationships in Black Sea sediments as indicators of environments of deposition. *Geochim. Cosmochim. Acta* **47**, 133–137.

Lewan M. D. (1983) Effects of thermal maturation on stable organic carbon isotopes as determined by hydrous pyrolysis. *Geochim. Cosmochim. Acta* **47**, 1471–1479.

Lewan M. D. (1984) Factors controlling the proportionality of vanadium to nickel in crude oils. *Geochim. Cosmochim. Acta* **48**, 2231–2238.

Lewan M. D. (1985) Evaluation of petroleum generation by hydrous pyrolysis experimentation. *Philos. Trans. Roy. Soc., Lond., Ser. A* **315**, 123–134.

Lewan M. D. (1987) Petrographic study of primary petroleum migration in Woodford Shale and related rock units. In *Migration of Hydrocarbons in Sedimentary Basins* (ed. B. Doligez). Éditions Tecnip, Paris, pp. 113–130.

Lewan M. D. (1993) Laboratory simulation of petroleum formation: Hydrous pyrolysis. In *Organic Geochemistry Principles and Applications* (eds. M. H. Engel and S. A. Macko). Plenum, New York, pp. 419–442.

Lewan M. D. (1997) Experiments on the role of water in petroleum formation. *Geochim. Cosmochim. Acta* **61**, 3691–3723.

Lewan M. D. and Henry A. A. (1999) Gas:oil Ratios for Source Rocks Containing Type-I, -II, - IIS, and -III Kerogens as Determined by Hydrous Pyrolysis. U.S. Geological Survey Open File Report 99-327, 34 pp.

Lewan M. D., Kotarba M. J., Curtis J. B., Więcław D. and Kosakowski P. (2006) Oil-generation kinetics for organic facies with Type-II and -IIS kerogen in the Menilite Shale of the Polish Carpathians. *Geochim. Cosmochim. Acta* **70**, 3351–3368.

Lewan M. D. and Maynard J. B. (1982) Factors controlling enrichment of vanadium and nickel in the bitumen of organic sedimentary rocks. *Geochim. Cosmochim. Acta* **46**, 2547–2560.

Lewan M. D. and Whitney G. C. (1993) The inhibitory effect of smectite on petroleum expulsion in hydrous pyrolysis experiments. In *American Chemical Society 205th National Meeting*, March 28-April 2, Denver, CO, Geochemistry Division Abstract No. 58.

Mango F. D. (1994) Role of transition-metal catalysis in the formation of natural gas. *Nature* **368**, 536–538.

Mango F. D. (1996) Transition metal catalysis in the generation of natural gas. *Org. Geochem.* **24**, 977–984.

Masel R. I. (2001) *Chemical Kinetics and Catalysis*. Wiley and Sons, New York, 952 pp.

Mayer W. and Piestrzyński A. (1985) Ore minerals from Lower Zechstein sediments at Rudna mine, Fore-Sudetic Monocline SW Poland. *Prace Mineralog.* **75**, 1–72.

Meissner F. F. (1978) Petroleum geology of the Bakken Formation, Williston Basin. In *Williston Basin Symposium*, Montana Geological Society 24th Annual Conference, pp. 207–227.

Meunier J. D. (1994) The composition and origin of vanadium-rich clay minerals in Colorado Plateau Jurassic sandstones. *Clays Clay Miner.* **42**, 391–401.

Montgomery S. L., Jarvie D. M., Bowker K. A. and Pollastro R. M. (2005) Mississippian Barnett Shale, Fort Worth basin, north-central Texas: gas–shale play with multi-trillion cubic foot potential. *Am. Assoc. Petrol. Geol. Bull.* **89**, 155–175.

Morel J. A. (1999) Use resistivity as indicator of source rock maturity. *Oil Gas J.* **97**(May 10), 72–74.

Olah G. A. and Molnár Á. (2003) *Hydrocarbon Chemistry*, Second ed. Wiley-Interscience, Hoboken, NJ, 871 pp.

Orr W. L. and Sinninghe Damsté J. P. (1990) Chapter 1 Geochemistry of sulfur in petroleum Systems. In *Geochemistry of Sulfur in Fossil Fuels* (eds. W. L. Orr and C. M. White), American Chemical Society Symposium Series 429, pp. 2–29.

Oszczepalski S. (1989) Kupferschiefer in southwestern Poland: sedimentary environments, metal zoning, and ore controls. In *Sediment-hosted Stratiform Copper Deposits* (eds. R. W. Boyle, A. C. Brown, C. W. Jefferson, E. C. Jowett and R. V. Kirkham). Geological Association of Canada Special Paper 36, pp. 571–600.

Palandri J. L. and Reed M. H. (2001) Reconstruction of in situ composition of sedimentary formation waters. *Geochim. Cosmochim. Acta* **65**, 1741–1767.

Passey Q. R., Creaney S., Kulla J. B., Moretti F. J. and Stroud J. D. (1990) A practical model for organic richness from porosity and resistivity logs. *Am. Assoc. Petrol. Geol. Bull.* **74**, 1777–1794.

Pearson M. J. (1979) Geochemistry of the Hepworth Carbonaceous sediment sequence and origin of the diagenetic iron minerals and concretions. *Geochim. Cosmochim. Acta* **43**, 927–941.

Peryt T. M. (1989) Basal Zechstein in southwestern Poland: sedimentation, diagenesis, and gas accumulations. In *Sediment-hosted Stratiform Copper Deposits* (eds. R. W. Boyle, A. C. Brown, C. W. Jefferson, E. C. Jowett and R. V. Kirkham). Geological Association of Canada, Special Paper 36, pp. 601–625.

Pieczonka J., Piestrzyński A. and Sawłłowicz Z. (2001) Copper–silver deposits in the Lubin-Głogów district (Poland). In *Mineral Deposits at the Beginning of the 21st Centuary, Geological Excursion Guide* (ed. Z. Sawłowicz), The Joint Sixth Biennial SGA-SEG Meeting, August 26–29, 2001, Krakow, Poland, pp. 5–50.

Piestrzyński A., Pieczonka J. and Głuszek A. (2002) Redbed-type gold mineralisation, Kupferschiefer, south-west Poland. *Mineral. Deposita* **37**, 512–528.

Püttmann W., Fermont W. J. J. and Speczik S. (1991) The possible role of organic matter in transport and accumulation of metals exemplified at the Permian Kupferschiefer formation. *Ore Geol. Rev.* **6**, 563–579.

Rimmer S. M. (2004) Geochemical paleoredox indicators in Devonian–Mississippian black shales, Central Appalachian Basin (USA). *Chem. Geol.* **206**, 373–391.

Robschlager K. H. W., Eleis C. A. and van Santen R. A. (1984) On the hydroisomerization activity of nickel-substituted mica-montmorillonite. *J. Catal.* **86**, 1–8.

Ruble T. E., Lewan M. D. and Philp R. P. (2003) New insights on the Green River petroleum system in the Uinta basin from hydrous pyrolysis experiments: reply. *Am. Assoc. Petrol. Geol. Bull.* **87**, 1535–1541.

Sawłowicz Z. (1990a) Primary copper sulphides from the Kupferschiefer, Poland. *Mineral. Deposita* **25**, 262–271.

Sawłowicz Z. (1990b) Native lead in the Polish Kupferschiefer. *N. Jb. Miner. Mh.* **1990**, 376–382.

Sawłowicz Z. (1993) Organic matter and its significance for the genesis of the copper-bearing shales (Kupferschiefer) from the Fore-Sudetic Monocline (Poland). In *Bitumens in Ore Deposits* (eds. J. Parnell, H. Kucha and P. Landis). Springer-Verlag, Berlin, pp. 431–446.

Sawłowicz Z., Gize A. P. and Rospondek M. (2000) Organic matter from Zechstein copper deposits (Kupferschiefer) in Poland. In *Organic Matter and Mineralization: Thermal Alteration* (eds. M. Glikson and M. Mastalerz), pp. 220–242. Hydrocarbon Generation, and Role of Metallogenesis. Kluwer Academic, Boston.

Schmoker J. W. and Hester T. C. (1990) Formation resistivity as an indicator of oil generation—Bakken Formation of North Dakota and Woodford Shale of Oklahoma. *Log Analyst* **31**, 1–9.

Sinfelt J. H. (1973) Specificity in catalytic hydrogenolysis by metals. *Adv. Catal.* **23**, 91–119.

Sinfelt J. H. (1991) Catalytic hydrogenolysis on metals. *Catal. Lett.* **9**, 159–172.

Sinfelt J. H., Carter J. L. and Yates D. J. C. (1972) Catalytic hydrogenolysis and dehydrogenation over copper–nickel alloys. *J. Catal.* **24**, 283–296.

Snowdon L. R. (2001) Natural gas composition in a geological environment and the implications for the processes of generation and preservation. *Org. Geochem.* **32**, 913–931.

Somorjai G. A. (1994) *Introduction to Surface Chemistry and Catalysis*. John Wiley and Sons, New York, 667 pp.

Su K-H., Shen J-C., Chang Y.-J. and Huang W.-L. (2006) Generation of hydrocarbon gases and CO_2 from humic coal: experimental study on the effects of water, minerals, and transition metals. *Org. Geochem.* **37**, 437–453.

Sun Y. and Puttmann W. (1997) metal accumulation during and after deposition of the Kupferschiefer from the Sangerhausen Basin, Germany. *Appl. Geochem.* **12**, 577–592.

Swift H. E. and Black E. R. (1974) Superactive nickel–aluminosilicate catalysts for hydroisomerization and hydrocracking of light hydrocarbons. *Ind. Eng. Chem. Prod. Res. Dev.* **13**, 106–110.

Turekian K. K. and Wedepohl K. H. (1961) Distribution of elements in some major units of the earth's crust. *Geol. Soc. Am. Bull.* **72**, 175–191.

Vieira Coelho A. C., Poncelet G. and Ladrière J. (2000a) Nickel, iron-containing clay minerals from Niquelândia deposit, Brazil. 1: Characterization. *Appl. Clay Sci.* **17**, 163–181.

Vieira Coelho A. C., Ladrière J. and Poncelet G. (2000b) Nickel, iron-containing clay minerals from Niquelândia deposit, Brazil. 2: Behavior under reducing conditions. *Appl. Clay Sci.* **17**, 183–204.

Wearing E. (1984) Occurrence of some Ni- and Sn-rich minerals in copper converter slag. *Mineral. Mag.* **48**, 243–249.

Whiticar M. J. (1994) Correlation of natural gases with their sources. In *The Petroleum System-from Source to Trap* (eds. L. B. Magoon and W. G. Dow). American Association of Petroleum Geologists Memoir 60, pp. 261–283.

Wodzicki A. and Piestrzyński A. (1994) An ore genetic model for the Lubin-Sieroszowice mining district, Poland. *Mineral. Deposita* **9**, 30–43.

Wolf M., Eckardt C. B., Hagemann H. W. and Püttmann W. (1989) Facies and rank of the Permian Kupferschiefer from the Lower Rhine Basin and NW Germany. *Int. J. Coal Geol.* **14**, 119–136.

Associate editor: Jeffrey Seewald